COINCIDENCE COUNTING TECHNIQUES FOR THE DETERMINATION OF ^{226}Ra CONCENTRATIONS IN WATER

BY

© DIANE MARTHA LOWE, B.Sc.

A Thesis

Submitted to the School of Graduate Studies

in Partial Fulfilment of the Requirements

for the Degree

Master of Science

McMaster University

April 1981

MASTER OF SCIENCE (1981) McMASTER UNIVERSITY
(Physics) Hamilton, Ontario

TITLE: Coincidence Counting Techniques For The Determination of ^{226}Ra Concentrations in Water

AUTHOR: Diane M. Lowe, B. Sc. (McMaster University)

SUPERVISOR: Dr. W. V. Prestwich

NUMBER OF PAGES: ix, 121

ABSTRACT

Three coincidence counting techniques for the assay of ^{226}Ra in water samples are evaluated and compared. The techniques are based on the detection of alpha-gamma, beta-gamma, and gamma-gamma coincident radiations. Samples were prepared by co-precipitating ^{226}Ra with barium sulphate. Details of this chemical procedure are presented in this thesis. The lower limit of detection, sensitivity to sample thickness, and system precision are investigated. Finally, two data analysis techniques, the method of Least Squares and the method of Maximum Likelihood, for determining -ray peak areas as applied to low counting rates, are discussed.

ACKNOWLEDGEMENTS

I wish to express my sincere appreciation to my research supervisor, Dr. Bill Prestwich, whose continual encouragement, enthusiasm and insight enabled this work to be completed. It is also a pleasure to express my gratitude to Alice Pidruczny for answering my numerous questions concerning chemistry and sample preparation, and for attempting the impossible: turning a physicist into a chemist.

Thanks also goes to Kenrick Chin and Ian Cunningham for their patience and help with the electronics and computer problems, and to Nick Barkman for proofreading the thesis.

There are many other people at McMaster I wish to specially thank for helping me through difficult times and making my stay here an educational and enjoyable one. Among these are Bill, Ed, Bob, Nick, Tom, Richard, Leo, Mike, René, ..., Wordstar, Pepper and Teddy Bears.

TABLE OF CONTENTS

TABLE OF CONTENTS

LIST OF ILLUSTRATIONS

LIST OF ILLUSTRATIONS

LIST OF TABLES

CHAPTER 1

INTRODUCTION

1.1 Introduction

Man is exposed to ionizing radiation in the environment from three major sources: cosmic rays, terrestrial radiation, and internal radiation. The primary contributor to the environmental radiation dose is terrestrial radiation, owing to radioactive elements in the earth. These elements are mainly members of the uranium and thorium series, and ^{40}K. Over the years the greatest interest has been directed towards two specific members of these series, radium and its daughter product radon. Radium has 13 known radioactive isotopes, ranging in atomic number from 213 to 230, and radioactive half-life from 1 msecond to 1600 years. Of these, ^{226}Ra, from the ^{238}U series, and ^{228}Ra, also known as mesothorium, from the ^{232}Th series, are the principle isotopes of concern to Health Physicists.

Much of the data on the health hazards of radium comes from the radium dial workers, those women who painted watch and clock dials approximately 50 years ago. When radium is taken into the body, it behaves chemically like calcium, and an appreciable fraction is deposited on bone surfaces and in areas of active bone turnover. Radium is known to induce malignancies of bone and malignancies arising in certain cavities in bone, such as the paranasal

sinuses and the mastoid air cells. These malignancies tend to occur long after the first exposure to radium, from approximately 7 to more than 50 years in the case of head carcinomas. The occurrence of malignancies is strongly correlated with radium intake. As a result of the radium dial worker cases, an equation has been derived that expresses the probability of developing a bone cancer as a function of radium intake[1].

Mining of uranium bearing ores began in the United States around 1898. It was known at that time that radioactivity was associated with the ore, but the potential health hazards were not suspected until about 1921, when the increased incidence of lung cancer in uranium mine workers was related to their exposure to ionizing radiation. The primary radiation dose received by the mine workers was from alpha particles resulting from the decay products of radium. Radium alpha decays to radon, an inert gas which subsequently decays to several alpha emitting daughters. These radon daughters become attached to dust particles in the air and are breathed in by the mine workers. Since these particles have a very short range in tissue and a high linear energy transfer, radiation injury to the respiratory tract can occur. This damage is generally of three basic types; tumours, atrophy of functional tissue, and increased susceptibility to other disease agents[2].

Now that the health hazards associated with the uptake of radium and its daughters by humans are relatively well known, stringent government controls as to the use and release of radium to the environment are enforced. Natural water usually contains dissolved radium which has been picked up from rocks and soil by leaching. However, the primary source of radium in the environment is waste from the uranium mining process. Once uranium has been extracted from the ore, usually by some acid leach process, the waste material must be disposed of. Extensive research has been carried out in the area of uranium mine waste disposal. In general, the waste products, such as solids, residues, leached liquors, and washes, are treated to precipitate out the solid materials, which are then contained in a specially designed area to prevent leakage into the ground water systems. The remaining fluids are monitored for radioactivity and then released to the environment if certain conditions are met.

With the recent increase in uranium mining in Canada, particularly in northern Saskatchewan, as well as an increase in the average grade of new deposits of uranium ore, accurate monitoring procedures for radium levels in water are essential. In Canada at the present time, the allowable concentrations in drinking water, as recommended by the International Committee on Radiation Protection,

(ICRP), for the two radium isotopes of primary interest, are:

3 pCi/liter for ^{226}Ra, and

10 pCi/liter for ^{228}Ra,

for the general public. Recently the ICRP issued new recommendations which increased these levels by a factor of 10(3).

It is evident, therefore, that an effective monitoring procedure must be capable of measuring radium concentrations at or below these specified levels. It is also desirable that the procedure be relatively simple and easily adapted to the analysis of a large number of samples in a short period of time.

The object of this thesis is to ascertain the feasibility of employing coincidence counting techniques for the measurement of ^{226}Ra concentrations in water. Three coincidence techniques are investigated; the first two are newly developed, the third, a γ-γ coincidence spectrometer, was originally developed for the assay of ^{226}Ra in soil samples(4). In this previous work it was determined that activities of 1 pCi/g could easily be measured. The details of these techniques will be discussed in a separate section. Briefly, the techniques are based on the detection of:

1) an α-γ coincident pair from the decay of ^{226}Ra to ^{222}Rn,

2) a β-γ coincident pair resulting from the decay of ^{214}Bi to ^{214}Po, and

3) a γ-γ coincident pair, also from ^{214}Bi.

The coincidence spectrometers consisted of a proportional counter for detection of α and β particles, and NaI(Tl) detectors for the measurement of γ radiation. In each case the coincidence γ-ray spectra were acquired and analysed. Peak areas were determined where necessary by fitting the background underneath the peak.

It is common practice in determining peak areas to use the Method of Least Squares, which assumes that for data from counting experiments, the shapes of the individual distributions governing the fluctuations in the observed data are nearly Gaussian. When the counting rates are low this assumption can lead to problems; therefore it was decided to compare results obtained using the above method to the results obtained using the Method of Maximum Likelihood with Poisson statistics.

Samples were prepared for this work from solutions containing known concentrations of ^{226}Ra. Radium was co-precipitated with barium sulphate onto filter discs suitable for counting. The sensitivity of each counting technique to sample thickness was investigated.

An important criteria when considering a measurement procedure of this nature is the lowest limit of detection. Therefore, the detection limit was determined for the three coincidence counting techniques.

Complete discussions of these details will be given later.

1.2 Review of Previous Work

There exist several commonly used techniques for the determination of 226Ra concentrations in water. Each method has specific advantages and disadvantages. A brief overview will be given here.

Non-specific gross alpha counting techniques may involve long waiting periods before counting and perhaps multiple counts at well separated intervals to determine interferences from other isotopes(5).

For alpha spectrometry, samples are prepared in a similar manner as for the present work. Radium is co-precipitated with barium sulphate and the final product is counted on a silicon surface barrier detector(6). Interferences from daughter products requires that samples be counted immediately after precipitation in order to obtain good resolution of the ^{226}Ra alpha peak. Results are also dependent on the thickness of the sample. Analysis of ^{226}Ra in the presence of other radium isotopes, such as

^{223}Ra and ^{224}Ra, results in spectra having overlapping peaks. The contribution of these nuclides to the ^{226}Ra peak must then be estimated by some method of peak fitting.

An innovative technique was suggested by D.N. Kelkar, and J.V. Joshi(7). In this method, radium was precipitated with barium sulphate in the presence of ZnS(Ag) scintillation powder. The samples were counted on a photomultiplier scaler assembly. Excellent efficiency can be obtained in such an integral sample-scintillator arrangement. The principle disadvantage with this technique is the counting procedure. Samples were counted at intervals of 30 minutes for the first three hours and then after 24 and 72 hours, in order to separate the radium and radon contributions.

By far the most sensitive method for determining 226Ra concentrations in water is the classical radon emanation technique, employing either an ionization chamber or a ZnS Lucas cell(8,9). The radium concentration is determined by measuring the ^{222}Rn formed. The water sample must be de-emanated before any quantitative analysis can begin, by having aged air bubbled through it for at least 20 minutes. This process is repeated in one or two days to allow the residual radon absorbed in the sample bottle to re-diffuse into the bottle air and escape during the second de-emanation procedure. When an ionization chamber is used

it must be evacuated and refilled with radon free air and the central electrode must be exchanged after each measurement, to retain a low background count. Therefore, the long waiting periods and labour involved render this technique impractical for fast processing of a large number of samples.

The application of coincidence counting techniques to the measurement of radium concentrations have been suggested previously(10,11). The method described in the first reference utilizes the α-γ transitions of ^{226}Ra and the β-γ transitions of ^{228}Ac for the measurement of ^{226}Ra and ^{228}Ra levels, respectively. No details concerning the counting system or results were given in this abstract. The second reference investigates the possibilities of the delayed coincidence method as applied to the analysis of several radionuclides. Natural mixes of radionuclides were analysed for the isotopes ^{214}Bi, ^{212}Bi, ^{219}Rn, and ^{220}Rn by using β-α and α-α delayed coincidences. The error in determining ^{214}Bi was stated as less than ± 15%.

The following chapters discuss in detail the experimental arrangements for the three coincidence counting techniques, the data analysis procedure, and the experimental results. Finally, variations on the basic coincidence counting technique for measuring ^{226}Ra levels in water samples are proposed.

CHAPTER 2

COINCIDENCE SPECTROMETRY

2.1 Theory

The ability to quantitatively measure low levels of radioactivity depends on many factors, such as the background counting rate, efficiency of the detection system, and source-detector geometry. It is customary, therefore to use a detector with high intrinsic efficiency and a source detector geometry with as large a solid angle as possible.

Consider, for example, the simple case where a radioactive source emits two γ-rays in cascade. Under such conditions, there is a non-vanishing probability that both γ-rays will strike the detector simultaneously and cause energy deposits in excess of the energy of either single γ-ray. This event may then not be detected in a spectrometric determination, and will result in an apparent loss in efficiency. The following analysis is largely based on a paper by W.V. Prestwich and T.J. Kennett(12).

The efficiency for observing a full energy event due to γ_1 may be written as,

$$\varepsilon = \rho_1 \varepsilon_1 \frac{\Omega}{4\pi} \left[1 - f_{12} \bar{W}_{12}(0) \varepsilon_2 \frac{\Omega}{4\pi} \right] \qquad 2.1$$

where: ρ_1 = photofraction;

ϵ_1 = intrinsic efficiency;

f_{12} = coincident intensity of γ_1;

$\overline{W}_{12}(0)$ = angular correlation function of the two γ-rays evaluated at 0° between them, since both photons are incident on the same detector, and averaged over the detector solid angle, Ω.

The term in brackets is a coincident summing correction factor, and represents the probability of not detecting γ_2 if γ_1 has been detected. With no summing, $\rho\epsilon_1\Omega/4\pi$ would be the efficiency of the full energy peak. For a single right cylindrical detector, the maximum obtainable geometry is 2π. Combining this with unit intrinsic efficiency, undistorted signals from one member of a coincident pair may result if the other member is emitted in the opposite hemisphere to the first. If this member was then detected in coincidence in a second detector, also having 2π geometry and unit intrinsic efficiency, no reduction in counting rate would result, assuming a 100% coincidence branching. The efficiency for a coincidence event is given by the product of the individual probabilities of obtaining a pulse in the full energy peaks times the angular correlation function evaluated at 180°. Thus,

$$\epsilon_{coin} = \rho\epsilon_1\epsilon_2 f_{12}\overline{W}_{12}(\pi)\,\frac{\Omega^2}{16\pi}, \qquad 2.2$$

where the two detectors are identical and arranged along a common axis.

For symmetry reasons the average angular correlation function, $\overline{W}_{12}$, is such that $\overline{W}_{12}(\pi) = \overline{W}_{12}(0)$, and is always near unity, so will be neglected in what follows. The ratio of coincidence to single detector efficiencies may be written as:

$$\frac{\varepsilon_{coin}}{\varepsilon} = \frac{\varepsilon_2 f_{12} \frac{\Omega}{4\pi}}{1 - \varepsilon_2 f_{12} \frac{\Omega}{4\pi}} \qquad 2.3$$

For the high efficiency condition of $\varepsilon_2 \Omega / 4\pi = 1/2$, the efficiency ratio in equation 2.3 approaches one if f_{12} is close to one. Considering a more complex case in which there are several coincident γ-rays, the coincidence intensity term becomes $\sum_r f_{1r}$, for correlations between no more than two members, and an average efficiency may be defined as:

$$\varepsilon_{ave} = \sum f_{1r} \varepsilon_r / \sum f_{1r} \qquad 2.4$$

Equation 2.3 then becomes:

$$\frac{\varepsilon_{coin}}{\varepsilon} = \frac{\varepsilon_{ave} \frac{\Omega}{4\pi} \sum f_{1r}}{1 - \varepsilon_{ave} \frac{\Omega}{4\pi} \sum f_{1r}} \qquad 2.5$$

In some cases, such as for ^{214}Bi, $\sum_r f_{1r}$ approaches unity, and as before, the ratio of equation 2.5 will also

approach unity if the high efficiency condition of $\epsilon_{ave}\,\Omega/4\pi = 1/2$ is achieved. Therefore the efficiency for coincidence detection relative to that for single -ray detection, owing to the coincidence summing effect, is higher than might be expected, even though high efficiency conditions are not normally reached in practice.

There is one important advantage to using a coincidence analysis system. Coincidence spectrometry may allow the detection of low intensity isotopes in the presence of high intensity interfering radiation, even when the isotope cannot be measured in a single detector arrangement. Signals from the background are randomly distributed in time and will not necessarily fulfill the coincidence conditions applied. It can be seen from equation 2.2 that the efficiency is proportional to the solid angle subtended at the source to the second order. This implies that the probability for detection of cascade radiation from remote points in the room is small. A further reduction in background occurs because cascade radiation originating outside the detector shielding will be attenuated by the product of the attenuating factors for each member of the cascade pair.

The background considerations discussed above also apply to the α-γ , β-γ coincidence systems, particularly for the α-γ system, since the background count rate is

almost zero.

2.2 Description of the Method

The first coincidence technique involves the direct decay of ^{226}Ra. The ^{226}Ra nucleus α decays to ^{222}Rn with a characteristic half-life of 1602 years. A corresponding de-excitation γ-ray from the first excited state of ^{222}Rn, located at 0.186 MeV[12], occurs with an intensity of 5.4%. The fact that the α decay and the emission of the de-excitation γ-ray are time correlated events may be used to advantage in a coincidence system. The α energies associated with the decay are 4.78(95%) MeV and 4.60(6%) MeV.

Similarily, the β decay of ^{214}Bi and subsequent emission of a de-excitation γ-ray may also be utilized in a coincidence system. ^{214}Bi is one of four short lived daughter products of ^{222}Rn. This nucleus decays 99.98% of the time to ^{214}Po, with a half-life of 19.7 minutes, and maximum β energies of 1.0(23%), 1.51(40%), and 3.26(19%) MeV. The first excited state of 214Po is located at 0.609 MeV[12], and the de-excitation γ-ray occurs with an intensity of 47%.

In over 90% of the decays which lead to the emission of the 0.609 MeV γ-ray, a preceeding coincident γ-ray is also emitted. This correlation is the basis for the γ-γ

coincidence technique. These preceeding γ-rays all have energies greater than 0.609 MeV The decay schemes for the three coincidence techniques are shown in figures 2.1 and 2.2.

2.3 Special Problems

2.3.1 Range of Alpha Paricles

As previously mentioned, some techniques for measuring ^{226}Ra levels require that the precipitate samples be relatively thin and of uniform thickness in order to obtain good α spectra. For the present work it was not expected that thickness of the samples would degrade the α energy sufficiently to cause problems in detection. The range of the predominant α particle, (4.78 MeV), in the $BaSO_4$ precipitate was calculated from the equation:

$$\frac{1}{R_{BaSO_4}} = \sum \frac{P_i}{R_{zi}}$$

where: P_i = weight fraction of each pure element in the mixture; and

R_{zi} = range in each pure element of atomic number Z, expressed in mg/cm^2.

R_z is given by the expression:

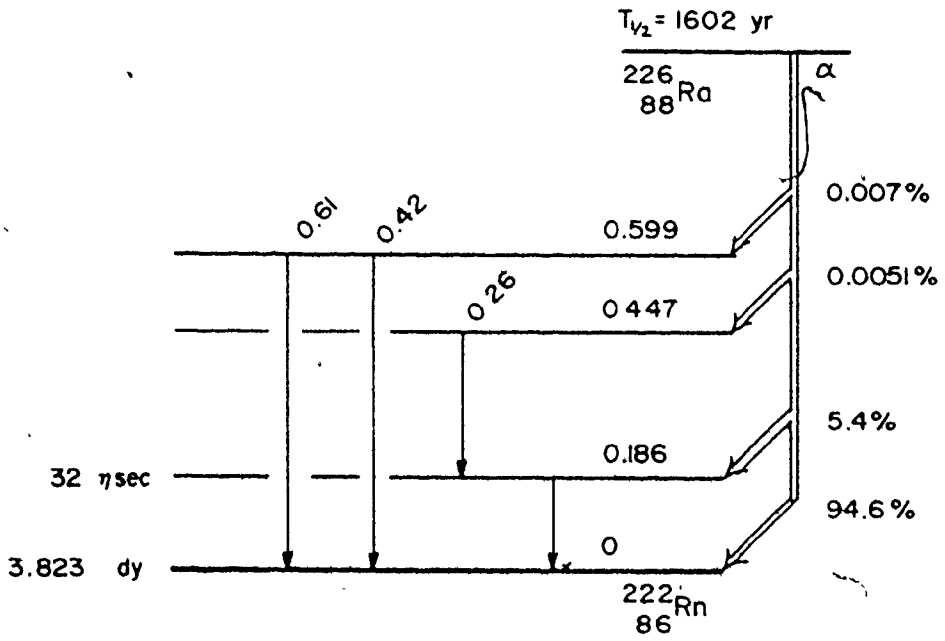

FIGURE 2.1 α-γ COINCIDENCE DECAY SCHEME

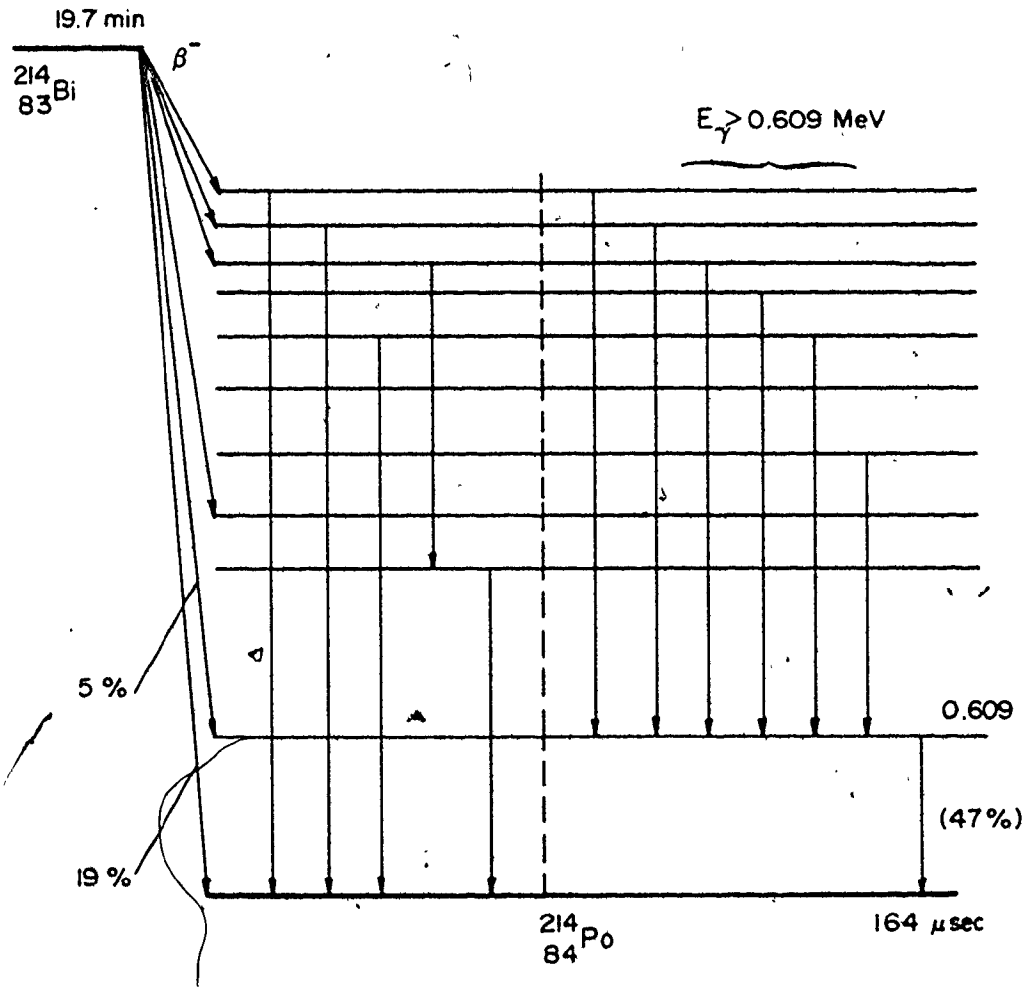

FIGURE 2.2 β-γ, γ-γ COINCIDENCE DECAY SCHEME

$$\frac{R_Z}{R_{air}} = 0.90 + 0.0275\ Z + (0.06 - 0.0086\ Z)\log_{10}(E/4),$$

where: $$R_{air} = (0.005\ E + 0.285)\ E^{3/2}\ \text{air}.$$

If $Z \leq 10$, the term $(0.90 + 0.0275\ Z)$, in equation 2.3, should be replaced by 1.00, and if $Z > 15$, R_Z is replaced by $(R_Z + 0.005\ Z)$.

The range of the 4.78 MeV particle from ^{226}Ra was calculated from the above expressions to be 5.61 mg/cm^2. The thickest sample counted was 2.89 mg/cm^2, based on the known quantity of barium used in the precipitation. Considering angular effects, the maximum effective thickness of the sample would be 4.09 mg/cm^2. If the proportional counter end window thickness of 0.8 mg/cm2 is included, the total thickness is still below the range of the 4.78 MeV α-particle

2.3.2 Interferences

In performing spectrometric analysis, an important consideration is the contribution from interfering isotopes to the spectra. Coincidence spectrometry is relatively insensitive to contaminants whose decays are characterised by the emission of a single γ-ray, α or β particle. However, within the uranium and thorium decay chains there exist many isotopes which α or β decay with the emission of one or several de-excitation γ-rays. Depending on the

concentration of these isotopes in the samples, and the relative intensities of these decays, a coincident pair could be detected. Even if the energy of the de-excitation γ-ray is different from the γ-ray of interest, Compton scattering in the sample and the response function of the NaI spectrometer both lead to the enhancement of low energy events, and therefore may contribute to the spectrum.

In the present work, as described in chapter 4, samples were prepared by co-precipitating radium with $BaSO_4$. As a result of this procedure, only radium isotopes from the uranium and thorium decay chains would appear in the samples. One member of the ^{235}U decay chain, ^{223}Ra, α decays to ^{219}Rn with the subsequent emission of several γ-rays; 0.149 complex(10%), 0.270(10%), and 0.33 complex(6%) MeV. However, the characteristic half-life of the ^{219}Rn is only 4.0 seconds, and thus any interferences from this isotope may easily be eliminated by delaying the start of the counting period. The ^{223}Ra decay scheme is outlined in figure 2.3.

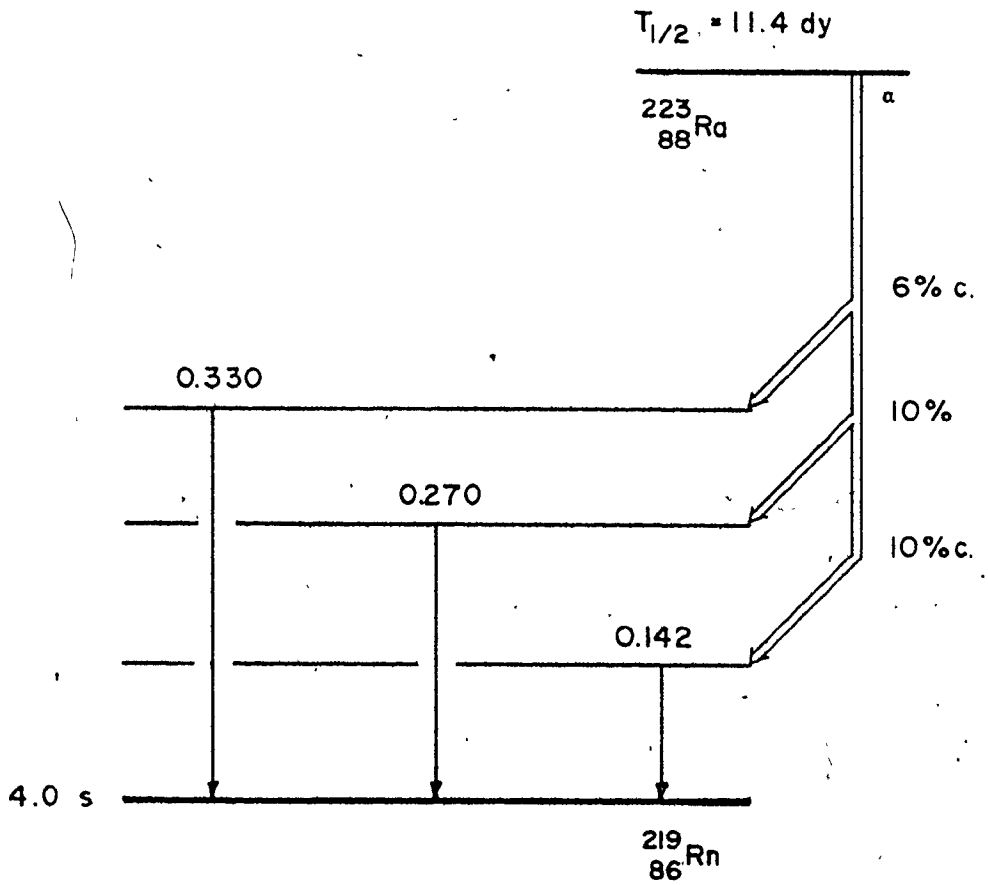

FIGURE 2.3 ^{223}Ra DECAY SCHEME

CHAPTER 3

THE EXPERIMENTAL SYSTEMS

3.1 Detectors

The experimental systems described in this work were set up to determine if coincidence counting techniques were suitable for measuring ^{226}Ra concentrations in water samples. Consequently, the detectors used in the spectrometers were chosen partially on the basis of convenience and availability. Good energy resolution was not critical; a more important consideration was the efficiencies of the detectors.

The γ-γ coincidence spectrometer consisted of two NaI(Tl) scintillation detectors, and the α-γ/β-γ coincidence spectrometer consisted of one NaI(Tl) detector paired with a gas flow proportional counter.

An important advantage in using a proportional counter is the ability to distinguish α and β particles; thus the same detector can be used for both the α-γ and β-γ coincidence systems. The α plateau, the region over which the count rate varies little with an increase in potential, occurs at a lower potential than for β particles. Alpha particles have a much higher specific ionization, and therefore pulses large enough to trip the discriminator are produced. As the potential is increased, the amplification factor becomes greater, and the pulses from the β particles

are registered. At this point the β plateau is reached. A good proportional counter should have a β plateau slope of $\leq 0.2\%$ per 100 volts[15]. A proportional counter has a very short resolving time and is very insensitive to radiation, making it ideal for α-γ/β-γ coincidence work.

Since the light output of a NaI(Tl) detector is proportional to the energy deposited in the crystal, the energies of the γ-rays from a radioactive source, as well as their intensities, can be measured, making the detector extremely useful in γ-ray spectrometry. Other factors which make this detector suited to coincidence work are the high efficiency and short pulse duration. The size of the NaI(Tl) crystal for a particular usage depends on the balance required between good time resolution and high efficiency; the former implying small crystal size, the latter, a large crystal size. For the coincidence arrangements described in this work, high efficiency was a major consideration.

A study was conducted to determine the optimum detector dimensions for maximum efficiency, given a fixed volume, V. In general, the efficiency of a detector is given by:

$$\varepsilon = \frac{1}{4\pi} \int p[L(\theta,\psi)]\, d\Omega$$

where: P_I = the probability of interaction between the γ-ray and the detector material,

$L(\theta,\varphi)$ = cord length in the detector material.

Then,

$$\varepsilon = \frac{1}{4\pi} \int_{\theta} \int_{\psi=0}^{2\pi} (1 - e^{-\mu L(\theta)}) \sin\theta d\theta d\psi$$

where: μ = absorption coefficient for the detector material.

Details of the analysis are given in Appendix A and will not be discussed here. The results of the computation indicate that for an absorption coefficient at an energy of 0.609 MeV, the maximum detector efficiency occurs when the radius is equal to 9.5 cm and the height is 1.22 cm, for a fixed volume of 347.5 cm, corresponding to a comercial 3 x 3 detector.

3.2 α-γ / β-γ Coincidence Spectrometer

3.2.1 Detector Arrangement

As previously discussed in section 3.1, the spectrometer used for both the α-γ and β-γ coincidence measurements consisted of one 7.5 cm high by 7.5 cm diameter NaI(Tl) detector to measure the γ radiation, and a flow proportional counter to detect the α and β radiation.

The NaI(Tl) detector was positioned along a vertical axis with the crystal section facing upwards, and was shielded by an annulus of lead, 4 cm thick by 11.5 cm high. This lead shield was surrounded by 0.3 cm of aluminum with an additional 3 cm on the bottom. The photomultiplier tube was shielded by 2 cm of lead.

The proportional counter used in the coincidence system was a Baird Atomic end window, gas flow counter. The detector was positioned directly above the NaI(Tl) detector, as shown in figure 3.1, and was completely covered by a dome shaped shield of lead, 2 cm thick by 10.5 cm high. Samples were inserted directly between the two detectors. A mixture of 10% methane, 90% argon was used as the counting gas, and the end window was a 0.8 mg/cm^2 Mylar film.

A count rate versus applied voltage curve was determined for the proportional detector, as shown in figure 3.2, in order to obtain the α and α plus β plateaus, as discussed in section 3.1. These plateaus were measured to

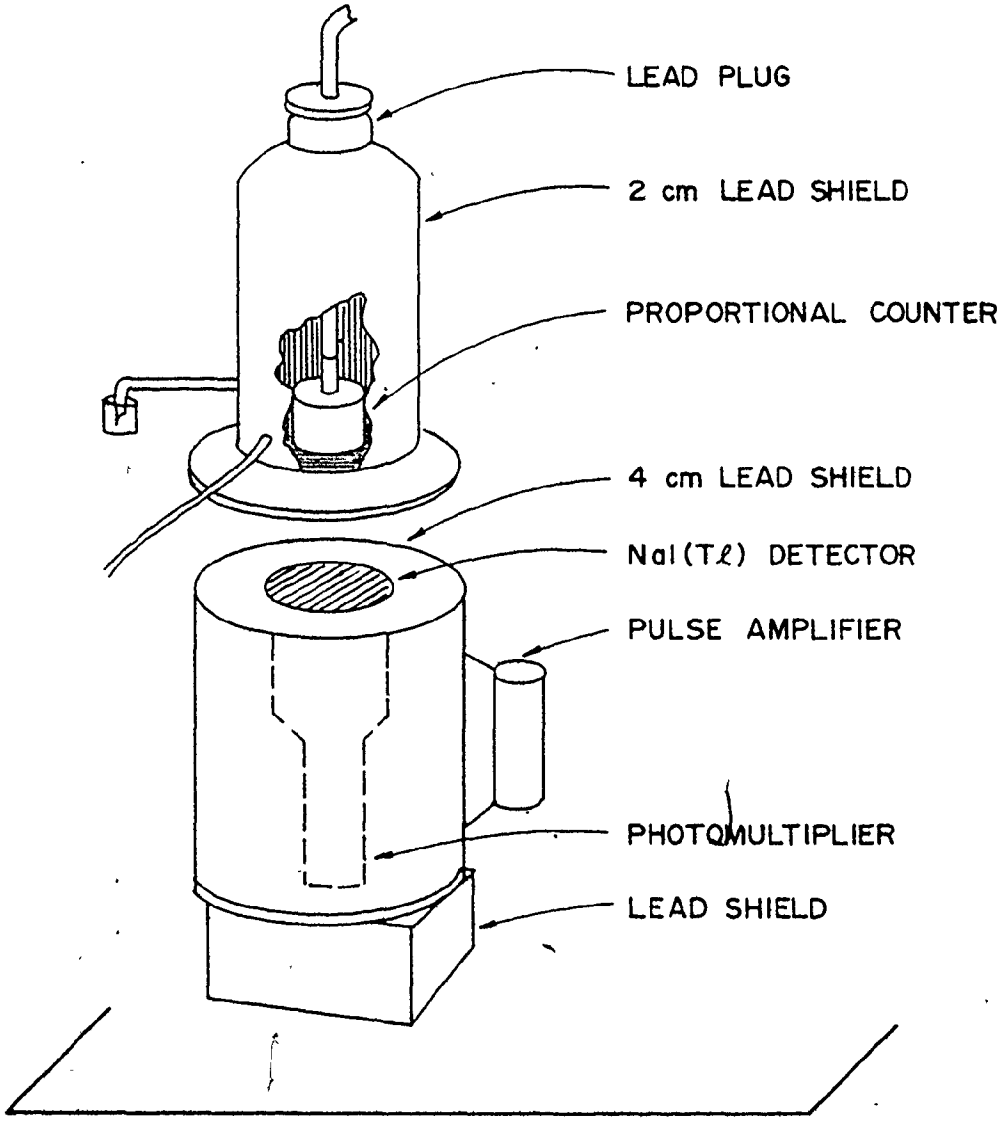

FIGURE 3.1 $\alpha-\gamma$ / $\beta-\gamma$ COINCIDENCE SPECTROMETER

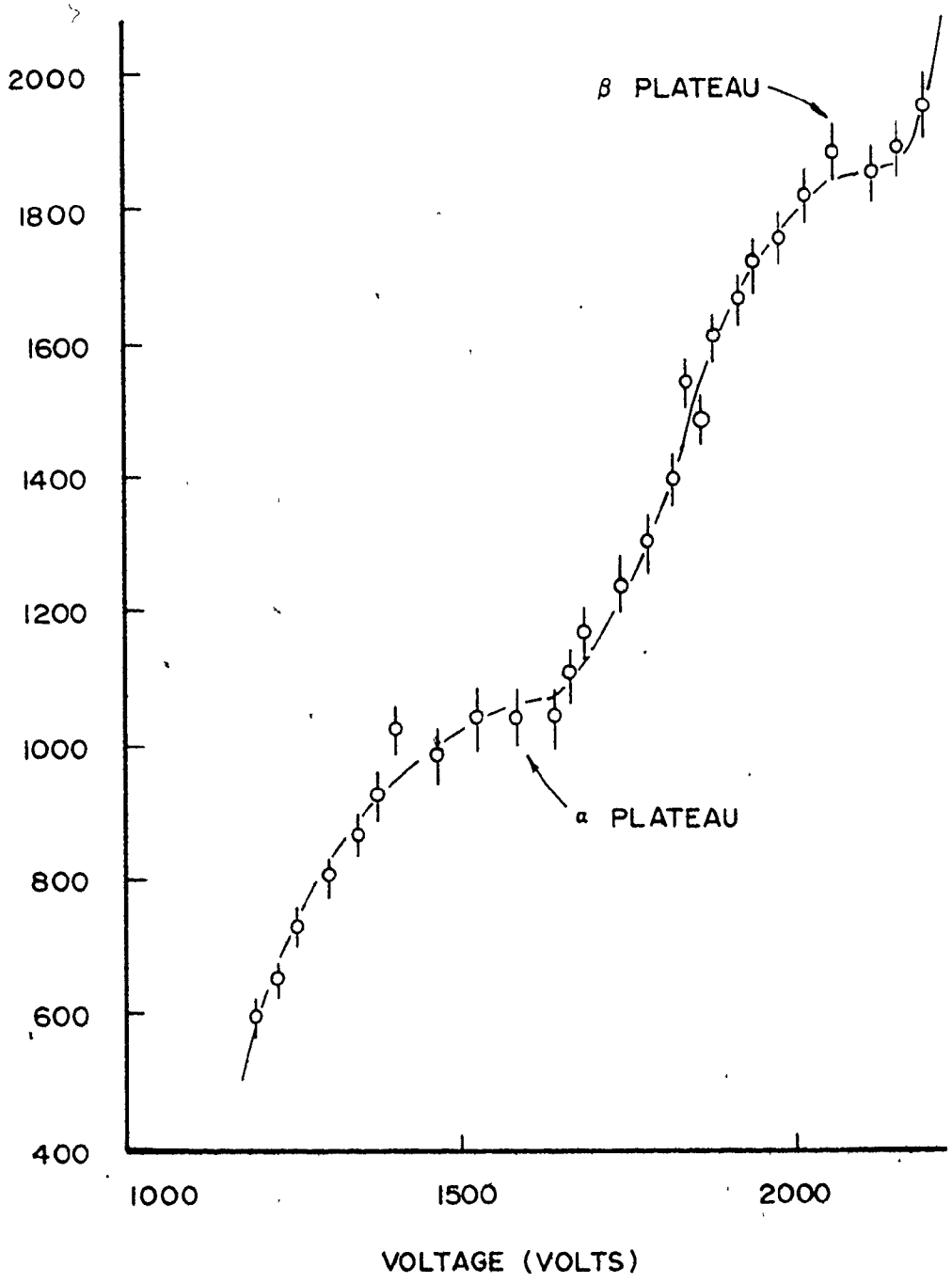

FIGURE 3.2 PROPORTIONAL COUNTER PLATEAU CURVE

occur at 1550 volts and 2100 volts, respectively. Neither of these plateaus were well defined, which meant that small fluctuations in the high voltage supply could cause significant changes in the sample count rate. This effect could be compensated for by running a standard each day that samples were run. This is further discussed in chapter 6.

3.2.2 The Electronic System

The coincidence system used in the present experiment is schematically outlined in figure 3.3. On the one side of the coincidence system, the pulses whose heights were proportional to the energy of the scintillation events in the NaI(Tl) detector were shaped, amplified, and fed to the input of a multichannel analyser, (MCA). The MCA was gated by the shaped, amplified, proportional counter pulses from the other branch of the coincidence system.

The anode pulse from the NaI(Tl) detector was integrated in a charge sensitive preamplifier and then processed in a linear delay amplifier system. Delay times were set such that the pulses from the two branches of the coincidence system met certain timing requirements dependent on the time distribution of the pulses. The output from the delay amplifier was recorded in a gated multichannel analyser.

Owing to the special nature of the proportional

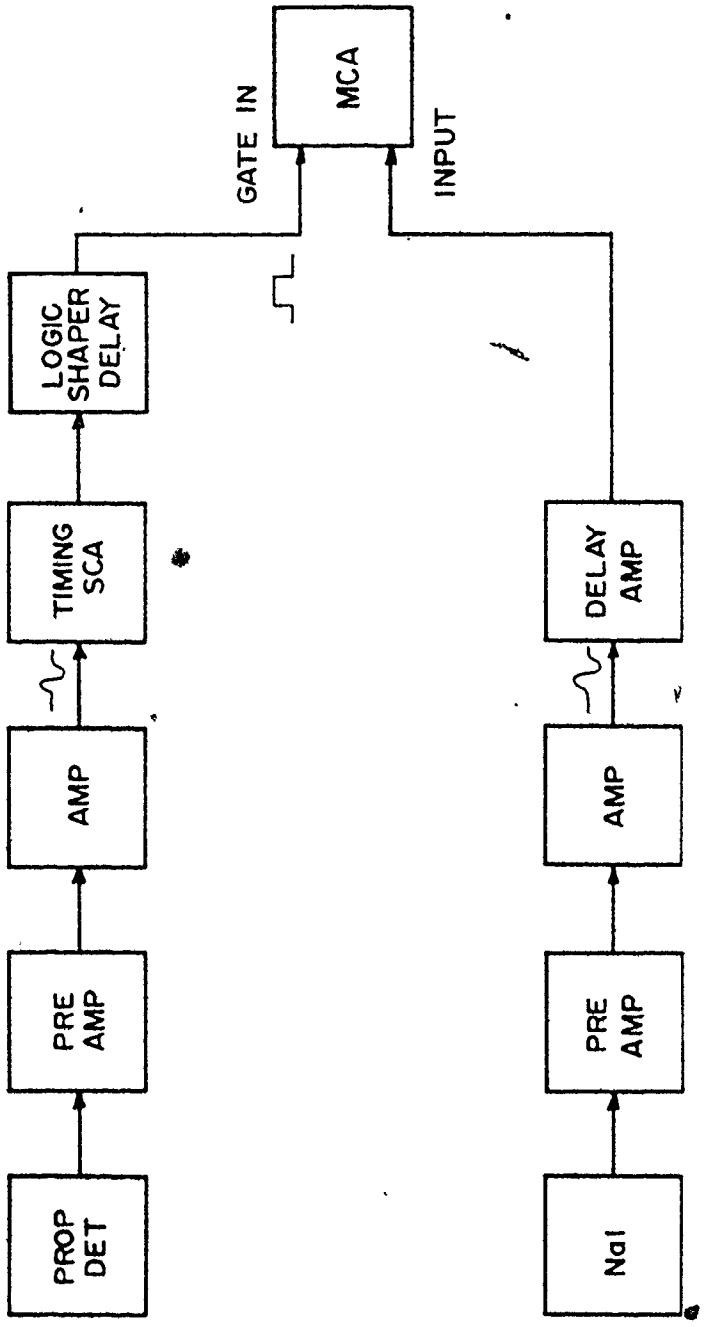

FIGURE 3.3 ELECTRONIC SYSTEM FOR $\alpha-\gamma/\beta-\gamma$ COINCIDENCE

counter pulses, high gain amplification was required. The electrons created as an α or β particle enters the sensitive volume of a proportional counter may be collected in a time less than 10^{-6} seconds, giving rise to a nearly negligibly wide impulse at the collector. The concurrent rapid drift of the positive ions, formed around the wire, towards the cathode, leads to a rapid increase in signal strength. The drift velocity of the positive ions is relatively high in the initial stages of development of a pulse, and thus the signal reaches half its maximum value in a time $t \simeq 10^{-3}T$, where T = the collection time for the positive ions, which is approximately less than 10^{-3} seconds. Therefore, in practice, the amplifier is designed to amplify linearly the initial stages of development of the signal, and to reject the later stages of slow rise to a maximum[14]. In the present arrangement, this rejection is not important.

The amplifier used for this work was a Tennelec TC 200 linear amplifier consisting of three stages; first differentiator, integrator, and second differentiator. The first stage reduced the duration of the pulse to a minimum value, consistent with accurate measurement, in order to minimize the probability of successive counts overlapping. The purpose in pulse shaping is to maximize the signal to noise ratio, (SNR), and to minimize the system resolving time. Since the noise is proportional to the bandwidth, the

bandwidth is minimized to get a good SNR. The second stage, the integrator, restricted the bandwidth of the signal, which slowed the rise of the pulse. The second differentiator reduced the duration of the undershoot to an acceptable level. In an AC coupled amplifier, the primary pulse is followed by an opposite polarity pulse, the undershoot, having an area equal to that of the primary pulse. The probability of successive pulses overlapping is relatively large if the undershoot has a long duration. At low count rates, however, the second differentiator may be switched out to increase the SNR, since the probability of overlapping pulses is small(16). The effects of the differentiating and integrating stages is illustrated in figure 3.4. For the present work, timing requirements are more important than achieving a good SNR. As further discussed in section 3.2.4, the coincidence γ-ray pulse height spectrum is collected and analysed, rather than the α or β coincidence spectra; thus the quality of the α and β spectra are not important.

The output signal from the amplifier was fed to a timing single channel analyser, (SCA), which produced a logic pulse output when the input pulse was within the desired energy "window", defined by adjustable upper and lower levels. This logic pulse was then fed to the input of a logic shaper and delay, in order to adjust the timing to

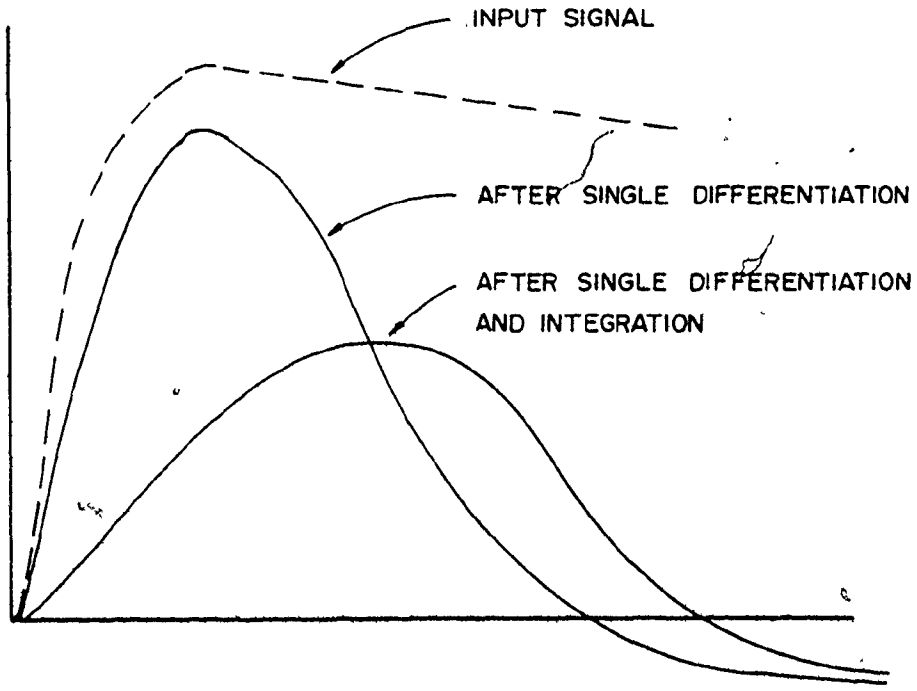

FIGURE 3.4 AMPLIFCATION OF PULSES

match the signal from the other branch of the coincidence circuit, and then to the gate input of a multichannel analyser, (MCA). The MCA therefore records the γ-ray spectrum in coincidence with either the α or β particle signals.

3.2.3 Time Distribution of Pulses

The time distribution of the pulses from the two detectors was measured, as shown schematically in figure 3.5. The NaI(Tl) detector signal, after passing through a linear amplifier and SCA, was used as the start pulse for the time to amplitude converter, (TAC), and the proportional counter signal, also after amplification and processing in an SCA, was used to stop the TAC. A TAC is basically a device which converts the time difference between two pulses to a pulse whose height is proportional to this time interval. If the output from the TAC is recorded in a multichannel analyser, the result is a plot of the number of start-stop coincidences as a function of time.

To calibrate the time scale, the negative SCA output from the NaI(Tl) channel of the coincidence system was used to start the TAC, as above, and the positive SCA output from the same channel was fed to a logic shaper and delay, whose fast output was used as the stop pulse. The logic delay was varied, and the TAC output was recorded in a MCA. The

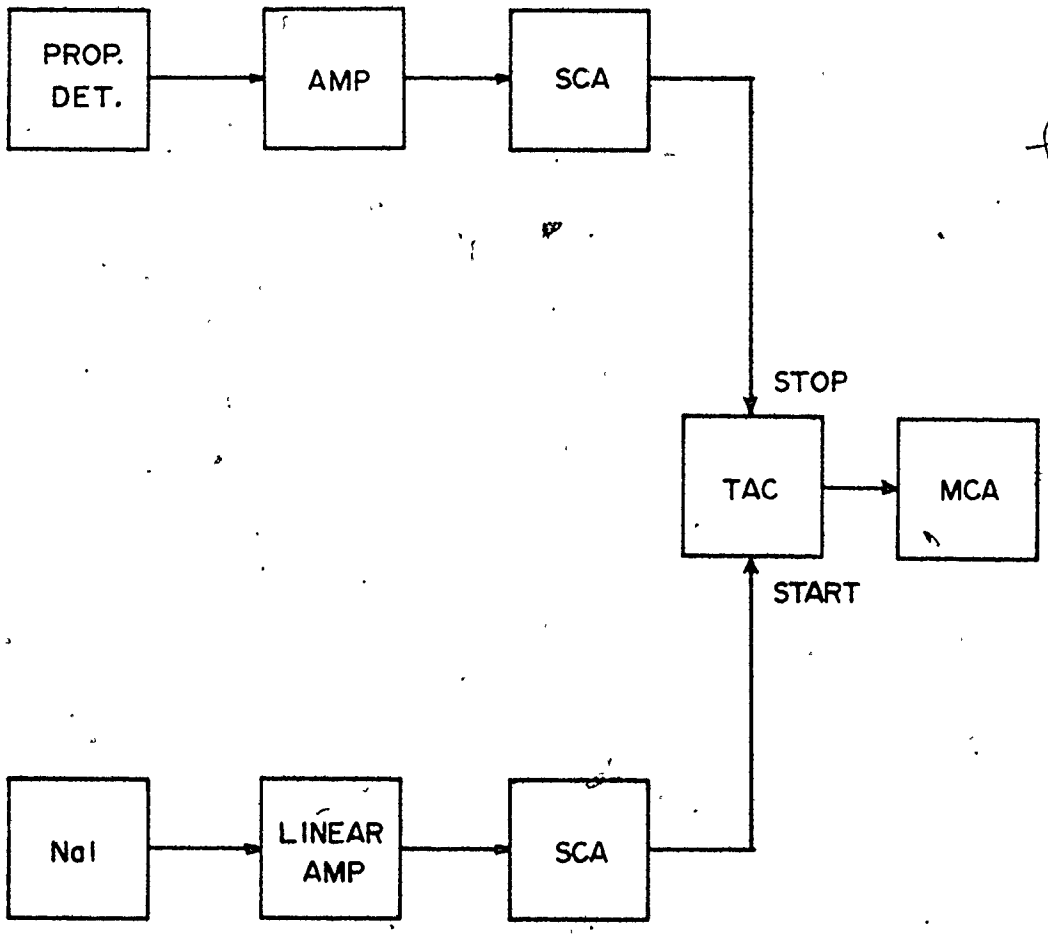

FIGURE 3.5 ELECTRONIC SYSTEM FOR PULSE TIME DISTRIBUTION MEASUREMENT

schematics are outlined in figure 3.6. A plot of time versus channel number is shown in figure 3.7.

The time distribution of the two pulses is illustrated in figure 3.8. The full width at half the maximum was 0.80 μsec, and the most probable time interval between the pulses from the two detectors was 3.0 μsec.

3.2.4 Measurement Procedure

Data were acquired in the coincidence mode in which the γ-ray pulse height spectra from the samples were recorded in the MCA, gated by the α or β signals. The upper and lower levels of the SCA on the α/β channel of the coincidence system were set such that the energy window was fairly wide.

Samples could be counted in the α-γ coincidence system directly after chemical preparation, whereas for β-γ coincidence counting, some period of time must elapse to allow the ingrowth of the 214Bi. This time interval depends on the activity of the sample. The correction factor for the ingrowth of the radon daughter products was calculated from the decay constants.

Background counts were taken over a period of 60,000 sec for the β-γ coincidence system, and 70,000 for the α - γ coincidence system. Table 3.1 shows a comparison of the background counting rates for the three coincidence counting

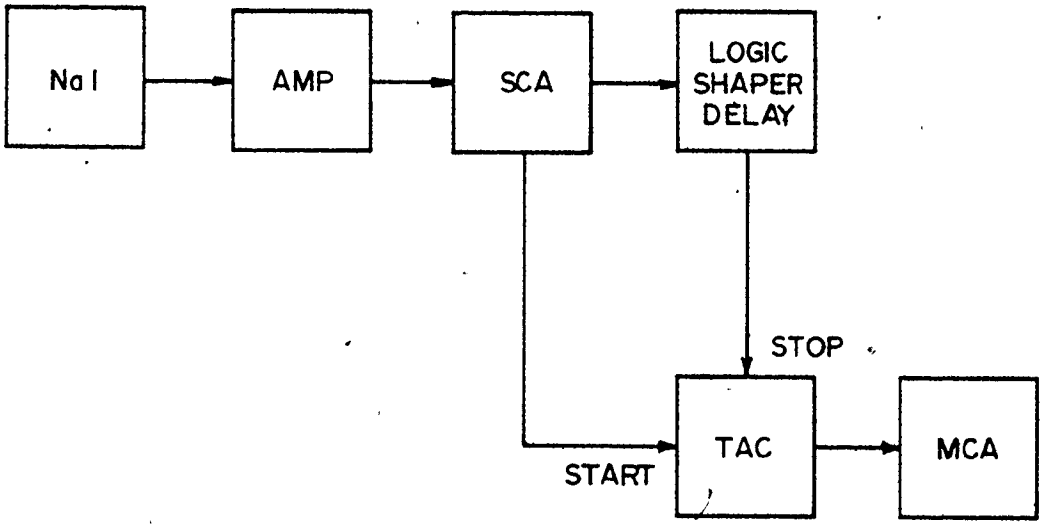

FIGURE 3.6 ELECTRONIC SYSTEM FOR TIME SCALE CALIBRATION

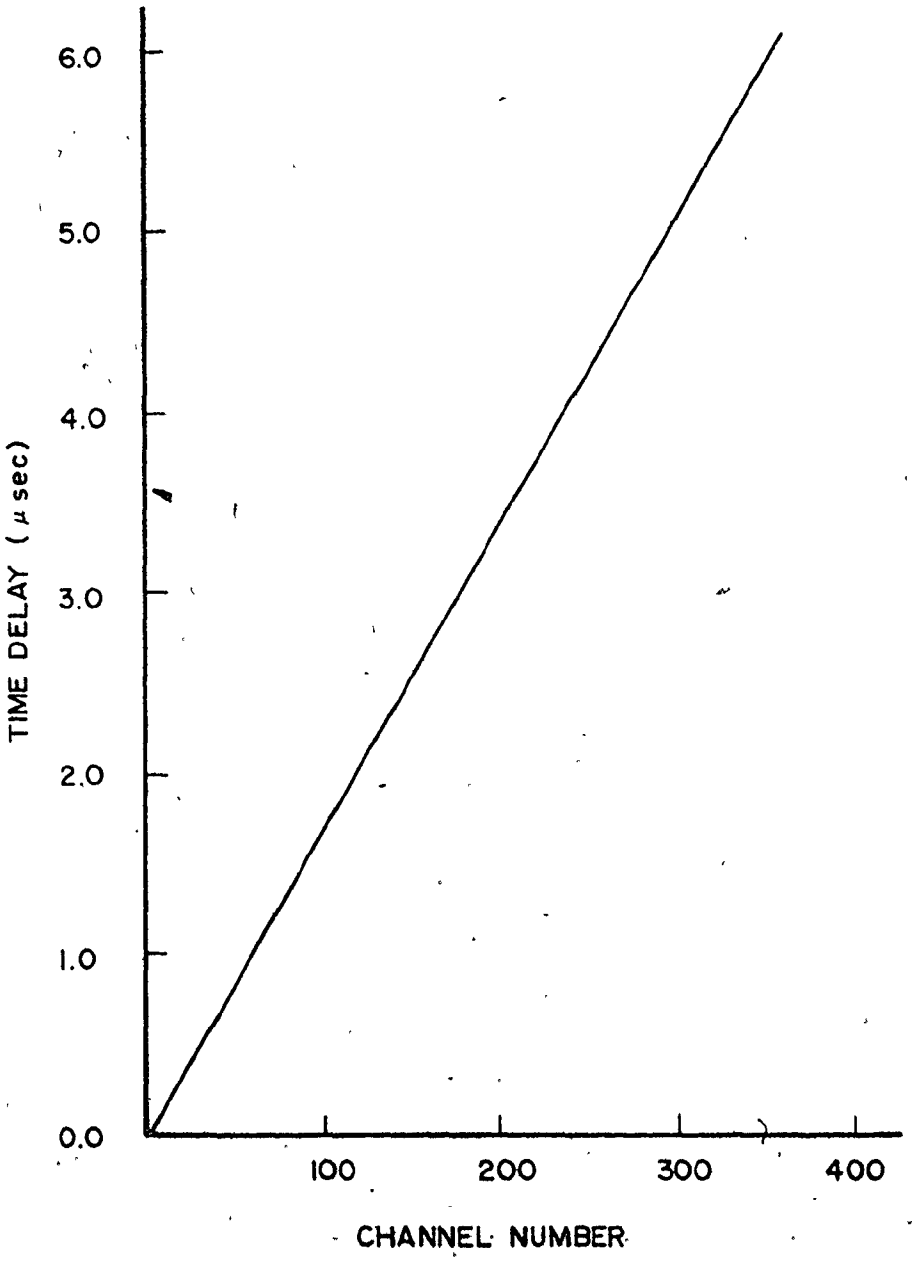

FIGURE 3.7 TIME CALIBRATION CURVE

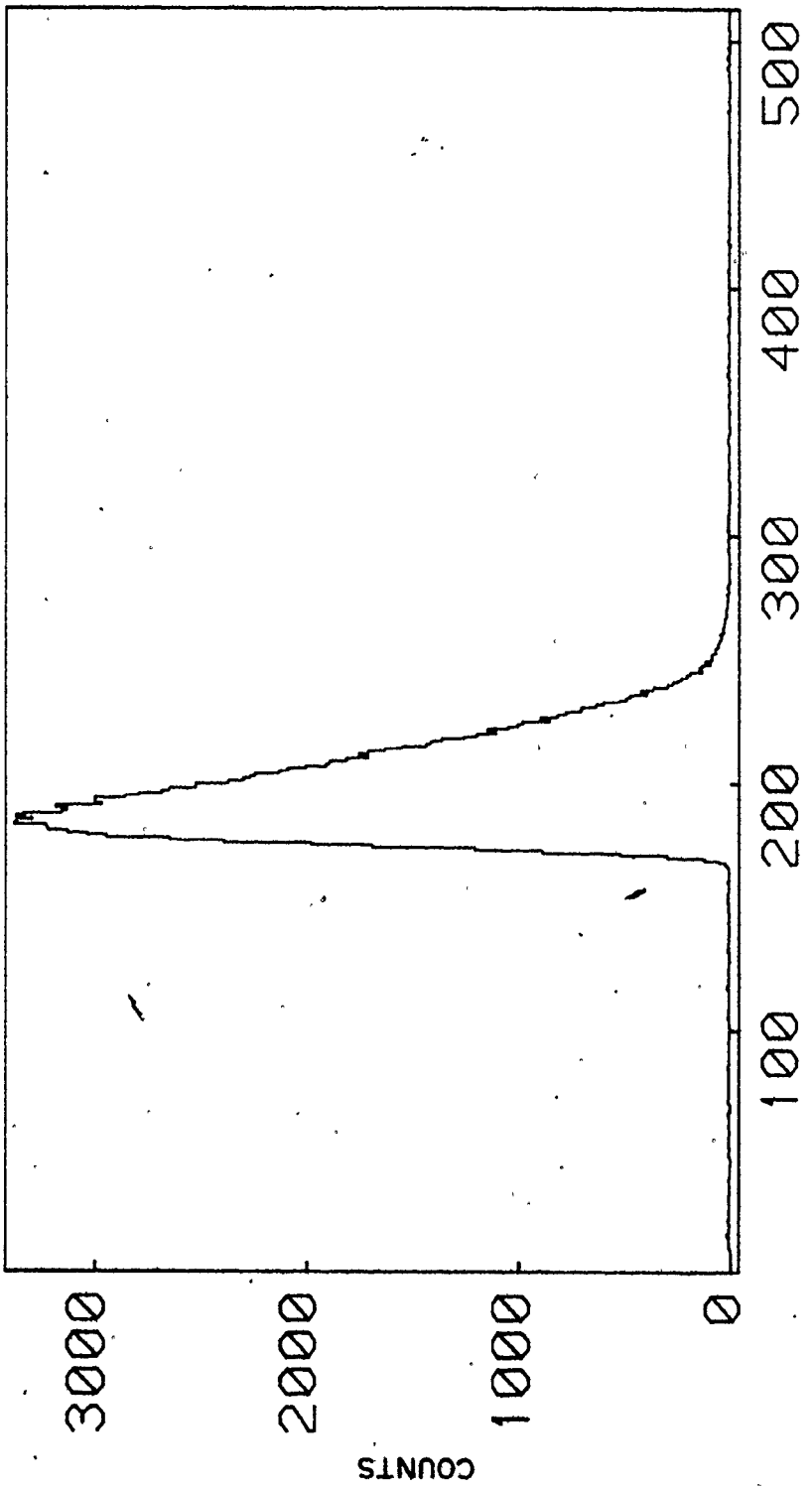

FIGURE 3.8 PULSE TIME DISTRIBUTION

TABLE 3.1

BACKGROUND COUNTING RATES (cts/sec)

$\alpha-\gamma$	$\beta-\gamma$	$\gamma-\gamma$
5.71×10^{-5}	3.35×10^{-3}	5.23×10^{-3}

TABLE 3.2

EFFICIENCIES (%)

$\alpha-\gamma$	$\beta-\gamma$	$\gamma-\gamma$
0.326	1.01	0.123

systems.

3.3 γ-γ Coincidence Spectrometer

3.3.1 Detector Arrangement

The gamma coincidence spectrometer consisted of two 7.5 cm high by 7.5 cm diameter NaI(Tl) detectors which were arranged along a common axis. An inner shield of 3 cm thick lead was molded to fit the crystal section and the photomultiplier base of the detector, and an outer annulus of lead 5 cm thick extended the length of the two detectors and enclosed the photomultiplier bases, as illustrated in figure 3.9. The detectors were spaced only a few millimeters apart such that the samples could be in close contact to the detectors, in order to achieve high efficiency conditions.

3.3.2 Electronics

The anode pulse from each detector was integrated with a charge sensitive preamplifier, and further processed in a double delay line linear amplifier. The zero-crossover point of the amplifier output pulse was used to mark the time occurrence of the two pulses. Timing single channel analysers were used to set pulse height range restrictions. The positive logic pulse of the channel of the coincidence system which was set to respond to all events of energy

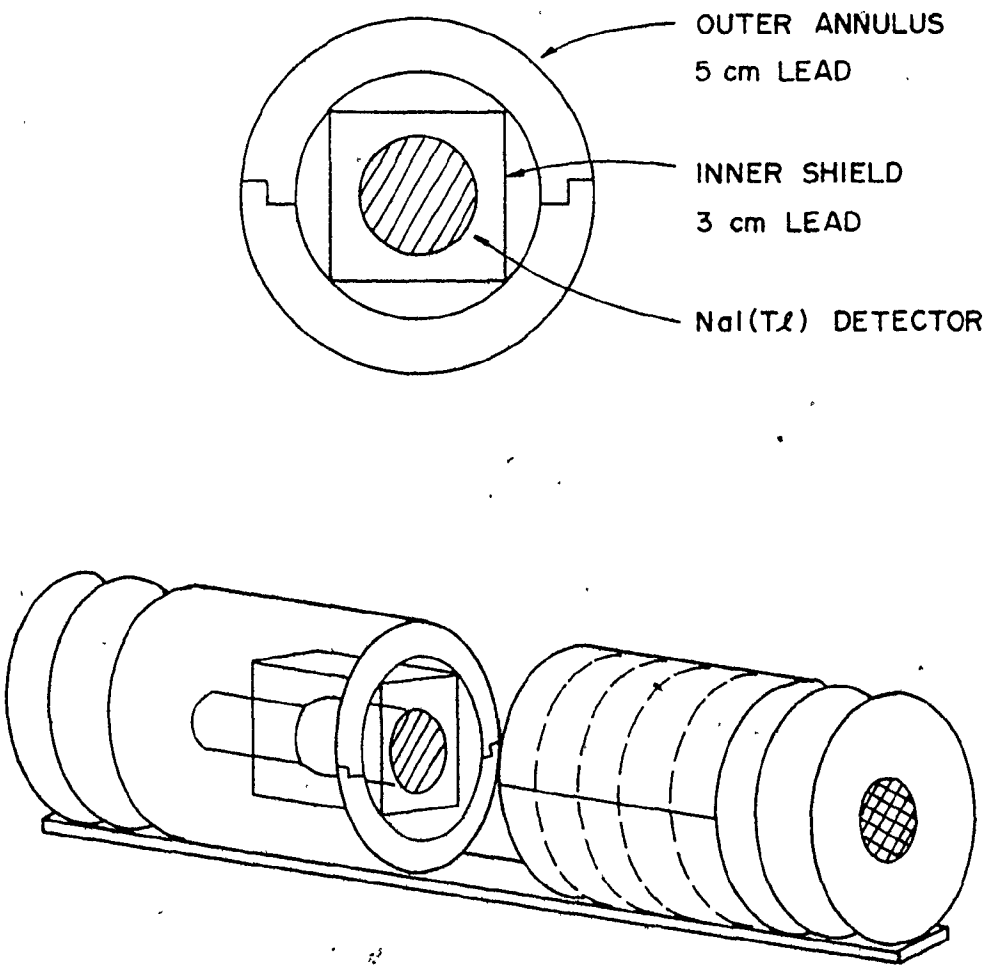

FIGURE 3.9 γ COINCIDENCE SPECTROMETER

greater than 0.609 MeV., was fed to a pulse stretcher and then coupled to a coincidence circuit with the negative output pulse from the SCA of the other channel of the system. The coincidence circuit consisted of an AND gate, a discriminator, and a linear gate. An output pulse from the AND gate resulted if the two input signals met specific timing requirements. This pulse was then passed through a discriminator, and the logic output pulse was used to gate the signal from one of the double delay line amplifiers. The coincidence pulse height spectrum from this channel was then recorded in a MCA. The variable delays in both the timing single channel analysers were adjusted such that the count rate from a ^{226}Ra standard source, at the output of the AND gate, was a maximum. A schematic outline of the system is shown in figure 3.10.

3.3.3 Measurement Procedure

The pulse height spectra of the samples were acquired under the coincidence condition in which the second detector responded to all events of energy greater than 0.609 MeV. In this arrangement the intense peak at 0.609 MeV., owing to the strong coincidence branching to the first excited state in ^{214}Po, was clearly visible.

With the energy range restrictions of this second detector as stated above, there exist two choices for the

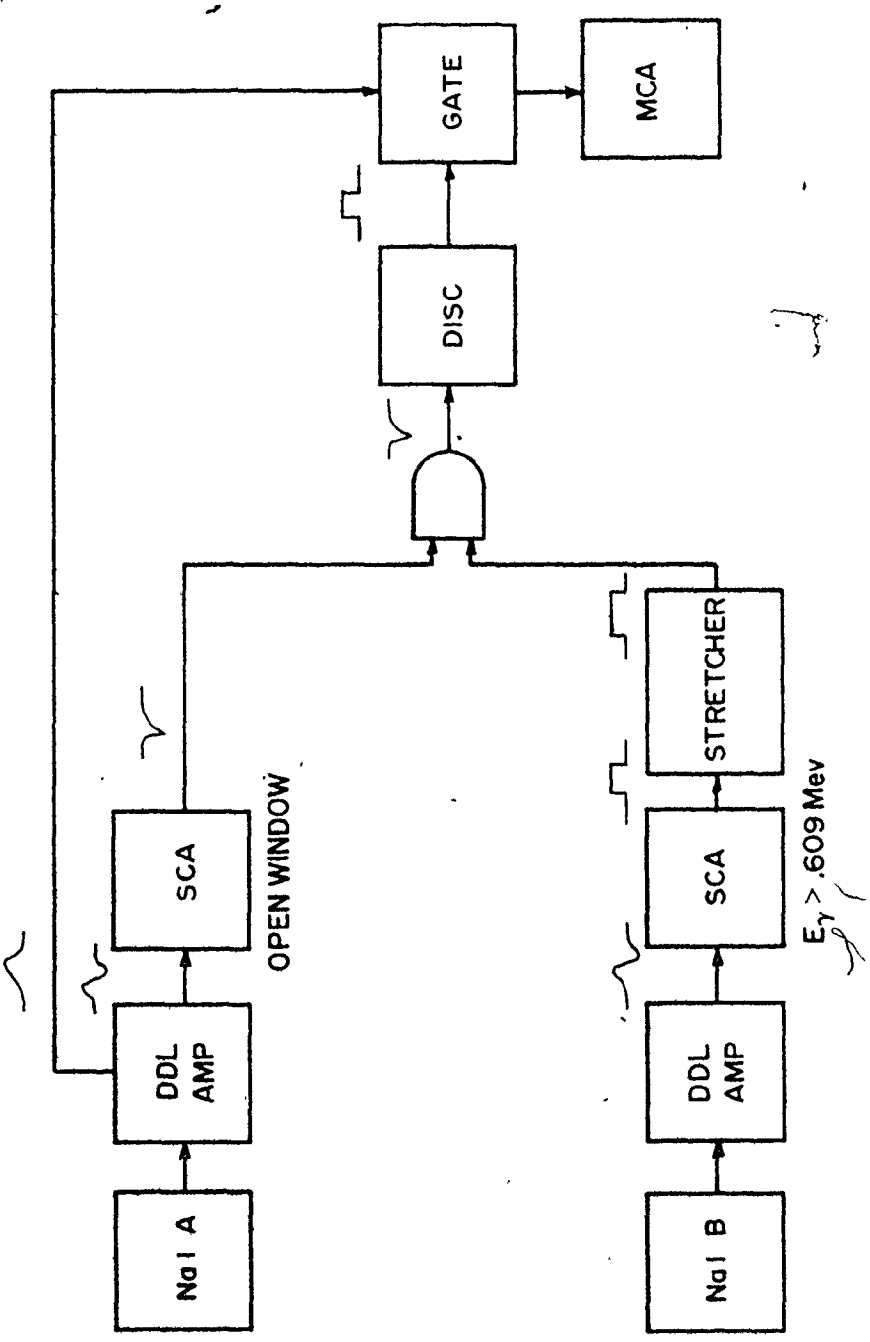

FIGURE 3.10 ELECTRONIC SYSTEM FOR γ-γ COINCIDENCE

energy restrictions of the first detector:

1) a narrow SCA window could be set such that this first detector responds only to the 0.609 MeV. event, or
2) the energy window could be left open to accept all events above the noise level.

However, in the first case, the fraction of counts appearing in the 0.609 MeV. peak due to the Compton continuum could not be determined, whereas in the second case, this fraction of events could be determined using background fitting techniques, which will be discussed in chapter 4.

Pulse height spectra of the samples could have been acquired in the reverse mode from above. An energy window could have been set such that the second detector responded only to the 0.609 MeV. event, and the coincident pulse height spectra collected from the other detector with no energy restrictions. In this way, various regions of the spectrum could be chosen for integration and analysis to maximize the signal to background ratio. This unfortunately results in a loss of efficiency, since the total counts would be reduced.

In γ-γ coincidence measurements, as for β-γ coincidence, corrections must be made for the ingrowth of the ^{222}Rn daughter products.

3.3.4 Contributions to Background

In attempting to count low level samples, it is important that the background counting rate be as low as possible. For singles counting, in a cave at ground level, the major contributors to the background are as follows[17]:

Cosmic rays (charged particle interactions)	55cpm
Cosmic rays ("soft" or cascade component)	120
Iron and Lead shield	110
5 in. phototube and preamplifier	100
Potassium-40 in crystal	30
Residual, unaccounted for	140
TOTAL	555cpm

The cosmic γ background may be reduced by employing an anti-coincidence shield. For the γ-γ coincidence system an attempt was made to determine the cosmic ray component of the background.

With the coincidence system set up such that one detector, A, responded to 0.609 MeV. events, and the other detector, B, responded to any events above the noise level, the percentage of the 0.609 MeV. energy "window" background of detector A, due to cosmic rays, was measured. To accomplish this, the gain of detector A was reduced by a large factor, and a coincidence pulse height spectrum from

detector B was acquired under the conditions described above. Basically, this gain change in detector A meant that higher energy events, (ie. events due to cosmic rays), were falling into the preset window. The cosmic ray background counts in this window were then equal to the number of counts in the entire spectrum of detector B. This count rate was determined to be $9.42 \cdot 10^{-3}$ counts per second. However, because of the change in the gain of detector A, the "window" width was also changed, and therefore the background count rate must be corrected for this effect. The correction factor was determined by finding the ratio of counts per channel in the region of the preset window at the normal gain, to the counts per channel in the higher energy region with detector B at 1/2 the gain. The correction factor was then equal to this ratio divided by the change in gain of detector A. This is illustrated in figure 3.11. Thus, the cosmic ray background count rate in the 0.609 MeV. window of detector A was $9.42 \cdot 10^{-3}$ (4.76/320) = $1.40 \cdot 10^{-4}$ counts per second. This contribution is so small that it is negligible.

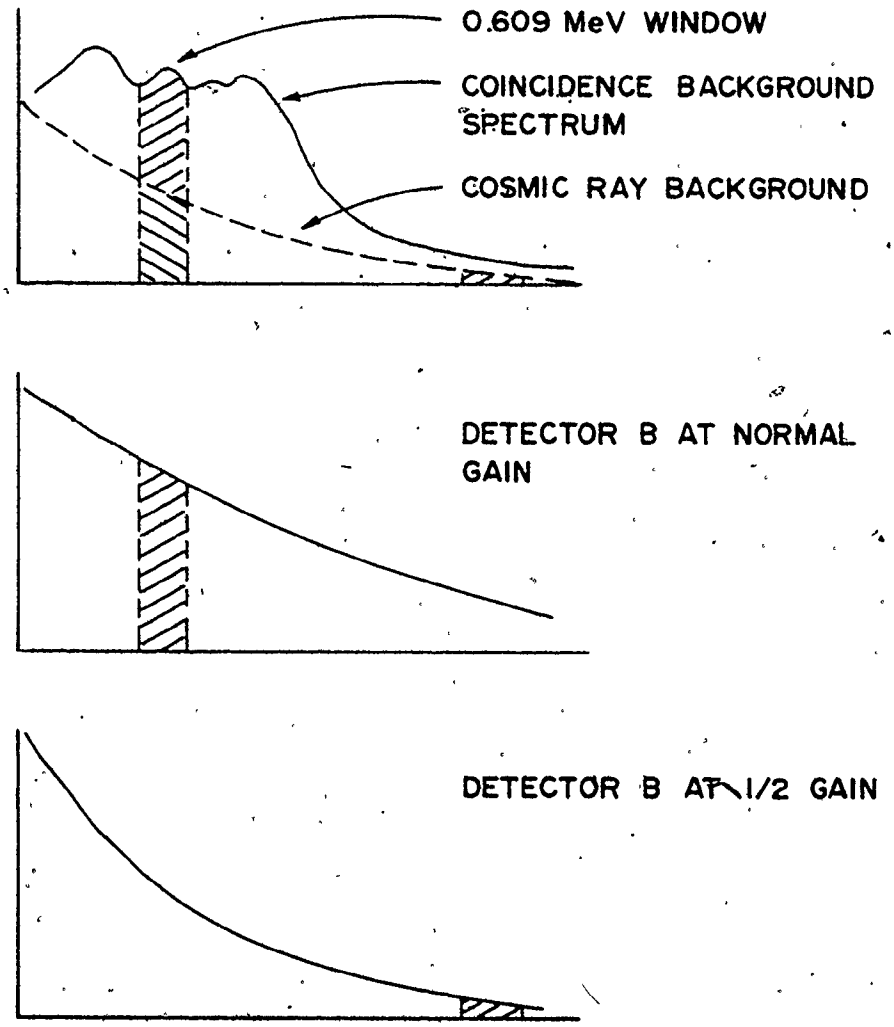

FIGURE 3.11 DETERMINATION OF COSMIC RAY BACKGROUND

3.4 Efficiency

The overall efficiencies of the α-γ, β-γ, and γ-γ coincidence systems were measured. The average counts per second of the ^{226}Ra-$BaSO_4$ precipitate standard were calculated from five separate measurements on each of the coincidence systems. The efficiency was then given by:

$$\text{eff} = \frac{(\text{average counts/sec of standard}) \cdot (1\ \text{Ci}/3.7\cdot10^{10}\ \text{dps})}{(\text{known activity of standard}) \cdot (1\ \text{Ci})}$$

The results of these calculations are shown in table 3.2.

3.5 Absolute Counting

It may be possible, in some cases, to do absolute counting of the samples. Consider a simple decay scheme, as illustrated in figure 3.12. The rate of γ_1 in detector A is given by:

$$R_1 = \epsilon_1^A F_1 D \quad ,$$

where: D = activity of the sample,

ϵ_1^A = efficiency of γ_1 in detector A.

Similarily, the rate of $_2$ in detector B is:

$$R_2 = \epsilon_2^B F_2 D \quad .$$

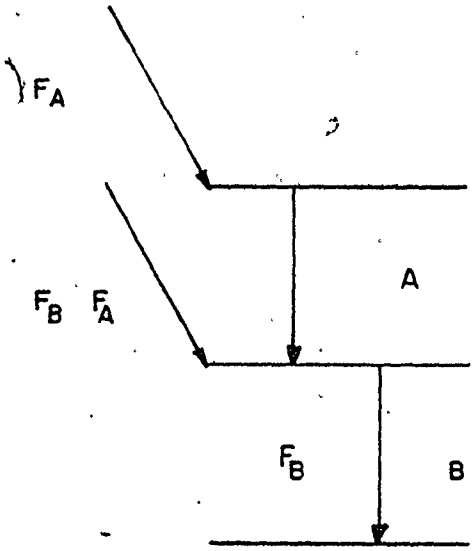

FIGURE 3.12 SIMPLE DECAY SCHEME

The coincidence rate is then given by:

$$R_{12} = \epsilon_1^A \epsilon_2^B F_1 D \quad .$$

Therefore;

$$\frac{R_1 R_2}{R_{12}} = \frac{(\epsilon_1^A F_1 D)(\epsilon_2^B F_2 D)}{(\epsilon_1^A \epsilon_2^B F_1 D)}$$

$$= F_B D \quad .$$

The result is significant in that all the efficencies have cancelled out.

However, when a radioactive source emits two γ-rays in cascade there is a finite probability that both will strike one detector simultaneously and cause energy deposits in excess of the energy of either single γ-ray, as previously discussed in section 2.1. Thus, the rates R_1 and R_2 must be corrected for this coincidence summing.

The measured rates are then given by:

$$R_1 = \epsilon_1^A (1-\epsilon_2^A) D$$

$$R_2 = \epsilon_2^B (1-\epsilon_1^B) D, \text{ and as before,}$$

$$R_{12} = \epsilon_1^A \epsilon_2^B D.$$

Therefore, the true rates are:

$$R_1^T = R_1 + R_{12}, \quad \text{if } \epsilon_i^A = \epsilon_j^B,$$

$R_2^T = R_2 + R_{12}$, and the activity of a sample is given by:

$$D = \frac{R_1^T \, R_2^T}{R_{12}} \cdot \frac{1}{F_2} \quad .$$

Even in a more complicated decay scheme, D will be proportional to $R_1^T R_2^T / R_{12}$, multiplied by an F factor which will be dependent on the particular branching ratios.

Absolute counting is feasible for the γ-γ coincidence system, providing that the activities of the samples are high enough such that the 0.609 MeV. peak is visible in the singles spectrum. If the samples are relatively fresh, the α-γ coincidence system may also be adapted to do absolute counting. However, in this case the samples must be counted before the alpha emitting ^{222}Rn daughters have grown in to any significant degree.

CHAPTER 4

CHEMISTRY

4.1 Introduction

A reliable routine procedure for the preparation of ^{226}Ra samples, suitable for α, β, and γ spectrometry, was required. The method followed for the present work was based on the method used by J.B. Zimmerman and V.C. Armstrong(18), adapted by A. Pidruczny(19) for use with radium stock solutions. Radium may be easily and quantitatively isolated as a sulphate, from a stock solution containing radium, by co-precipitation with a small mass of barium as carrier. The final precipitate may be dried and mounted in a form suitable for α, β, and γ counting.

The procedure used for the present work is discussed in detail in the following section. Since all samples prepared for this work were made from small volume stock solutions, the precipitation procedure differs slightly from that which would be used for unknown samples whose volumes would generally be greater than one liter.

4.2 Sample Preparation

To a 100 ml. beaker in a fumehood was added 20 ml. H_2O, 40 mg Pb^{+2}, and approximately 0.5 mg Ba^{+2}. The amount of barium was varied in order to test the sensitivity of the counting systems to sample thickness. A relatively large mass of lead ensures good barium recovery during its separation from other elements. If a large mass of barium were instead used, the resultant precipitate would be too thick to be alpha counted. The addition of the lead also ensures the removal of any radiogenic lead resulting from the daughter products of ^{226}Ra. J.B. Zimmerman and V.C. Armstrong[18] found that the radium recovery was independent of the mass of lead carrier over the range 10 to 100 mg. Barium tracer studies also conducted in this work determined that for a lead carrier of 40 mg and barium carrier of 0.5 mg, the barium recovery was 90%. Five ml. of EDTA solution from a 0.25 M stock solution, 8 M NH_4OH drop by drop until a pH 9 was reached, checked with indicator paper, and 1 gm. of ammonium sulphate, $(NH_4)_2SO_4$, were added. The EDTA solution, at a pH of 9, complexes the Ba, Ra, and Pb, owing to the following competing reactions:

$$1)\ Ba^{+2} + EDTA \longrightarrow BaEDTA$$

$$2)\ Ba^{+2} + SO_4^{-2} \longrightarrow BaSO_4\ ,$$

with similar competing reactions for the Ra and Pb. The

outcome of these competing reactions depends on the values of the reaction constants for each process. These values are given below[20]:

	K_{SP}
$BaSO_4$	6.31×10^{-10}
$RaSO_4$	2.51×10^{-10}
$PbSO_4$	1.00×10^{-7}

K_{MY}

Conditional Stability Constant

BaEDTA	pH 4	-----
	9	2.51×10^{6}
PbEDTA	pH 4	2.51×10^{9}
	9	1.58×1015

K_{SP} is the solubility product constant, and K_{MY} is the reaction constant for the formation of the EDTA complex. At pH 9 the K_{MY} values for the Ba, Ra, and Pb are such that the EDTA reactions are dominant, and the solution contains BaEDTA, RaEDTA, and PbEDTA with excess SO_4^{-2}.

The mixture was then stirred gently with a magnetic bar and approximately 8 drops of a 0.1% solution of bromocresol green indicator were added. The acidity was then adjusted to pH 4 by adding glacial acetic acid drop by drop until a colour change from blue to green occured. The change in the pH of the solution affects the K_{MY} values for

the reactions. The K_{MY} value for the formation of PbEDTA remains very large, whereas the K_{MY} values for the formation of BaEDTA and RaEDTA are negligible. Thus the dominant reactions for Ba and Ra become:

$$Ba^{+2},\ Ra^{+2} + SO_4^{-2} \longrightarrow Ba,\ RaSO_4.$$

Therefore the $RaSO_4$ and $BaSO_4$ precipitate out of the solution, leaving behind the PbEDTA. The solution was stirred gently for one to two hours to ensure complete precipitation, and then filtered with a small volume, (15 ml.), funnel, onto a 25 mm. diameter, RAWG millipore filter disc. The funnel was washed with a small volume of 50% EtOH to reduce the creep of the precipitate up the filter chimney wall. Care was taken to ensure a uniform distribution of the precipitate over the filter disc. The filter was then dried under an IR lamp and the filtrate was discarded.

For natural water samples containing unknown levels of ^{226}Ra, large volume samples, (greater than one liter), are generally treated. An initial concentration of the sample is effected by the dropwise addition of concentrated H_2SO_4 to the water sample in the presence of Ba and Pb carrier. The initial mixed precipitate is then redissolved in a small volume of EDTA (pH 9) solution. The pH conditions are then altered to effect the precipitation of $Ba,RaSO_4$ in a form suitable for counting.

For the present work, samples were prepared from two

stock solutions, one containing approximately 1 nCi per ml of ^{226}Ra, and the other containing approximately 10 pCi per ml. The amount of barium carrier used in the precipitation of radium was varied from 0.5 mg Ba^{+2} to 3.5 mg Ba^{+2}.

All samples were mounted on the back of thin, 7.5 cm. diameter aluminum discs with 2 cm. holes cut in the centers, to facilitate the positioning of the samples in the counting systems.

A standard was prepared from a 1 nCi per ml. ^{226}Ra stock solution, with 2.5 mg of barium as carrier. In a separate experiment, this sample was counted in a standard geometry using a 7.5 cm by 7.5 cm diameter NaI(Tl) spectrometer. The spectrometer was in turn calibrated using a 0.0993± 10% μCi 226Ra standard obtained from the Radiochemical Center, Amersham, England.

CHAPTER 5

DETECTION LIMIT

When a measurement process is being compared with another, an important consideration is the lower limit of detection for the two processes. Various mathematical expressions and widely ranging terminology are used as definitions for the limit of detection. The most commonly used definitions have been calculated for the hypothetical case in which a pure gamma emitter is counted over a specific time interval with a detector of a given efficiency. In this instance, the detection limit is dependent on the background counting rate. Several definitions may then be applied; 10% of the background, the background standard deviation, or a multiple of it. Since each definition involves the background counting rate, greater sensitivity may be achieved by maintaining this rate as low as possible. It is in this respect that coincidence counting techniques become important, as the background counting rates are extremely low.

In the present work, the definition of detection limit is as discussed in an article by Currie[20]. In this article, a distinction is made between three levels:

1) the decision level, or critical level, L_C;
2) the detection limit, L_D;
3) the limit for quantitative determination, L_Q.

To be detected, an observed signal must exceed the critical level, L_C. The decision "detected", due to the statistical nature of the measurement, is subject to two kinds of errors:

1) a decision that the activity is present when it is not;
2) a decision that the activity is absent when it is present.

The probability of making these errors depends on L_C and the sample activity. If the observed signal is sufficiently large, the probability of making these errors is negligible, and a minimum activity, L_D, can be defined. The determination limit, L_Q, allows a quantitative result sufficiently close to the true value to be obtained.

Values for L_C, L_D, and L_Q, as defined by Currie, are shown in table 5.1 for the case of paired observations and a well known blank. Paired observations implies that the background was counted immediatley after the sample, for the same length of time, and a well known blank is a background count determined over a long period of time such that the background provides a negligible standard deviation compared to that of the sample plus blank. These levels have been derived for measurements in which it was assumed that the probabilities for risk a) and for risk b) are 5 percent, and

To compare the detection capabilities of the three coincidence counting techniques, the detection level, L_D, was calculated as a fuction of time. The detection level is given by:

$$L_D = 3.29 \sqrt{R_B T} \cdot (1/\epsilon) ,$$

where: R_B = the background counting rate determined from a well known blank;

T = the counting time;

ϵ = the detection efficiency.

Thus:

$$\frac{L_D(t)}{T} = 3.29 \frac{R_B}{T} \cdot 1 ,$$

and the limiting detection activity is given by:

$$A_D = \frac{L_D}{T \; 3.7\times10^{-2}((\text{cts/sec})/\text{Ci}))} .$$

Values of R_B and for the α-γ, β-γ, and γ-γ coincidence systems are shown in table 5.2, and graphs of A_D as a function of time are shown in figure 5.1.

TABLE 5.1

DETECTION LIMIT

	L_C	L_D	L_Q
PAIRED OBSERVATIONS	$2.33\,\sigma_B$	$4.65\,\sigma_B$	$14.1\,\sigma_B$
WELL KNOWN BLANK	$1.64\,\sigma_B$	$3.29\,\sigma_B$	$10\,\sigma_B$

TABLE 5.2

EFFICIENCY AND BACKGROUND RATES

	$\alpha-\gamma$	$\beta-\gamma$	$\gamma-\gamma$
R_B (cts/sec)	5.71×10^{-5}	3.35×10^{-3}	5.23×10^{-3}
E (%)	0.326	1.01	0.123

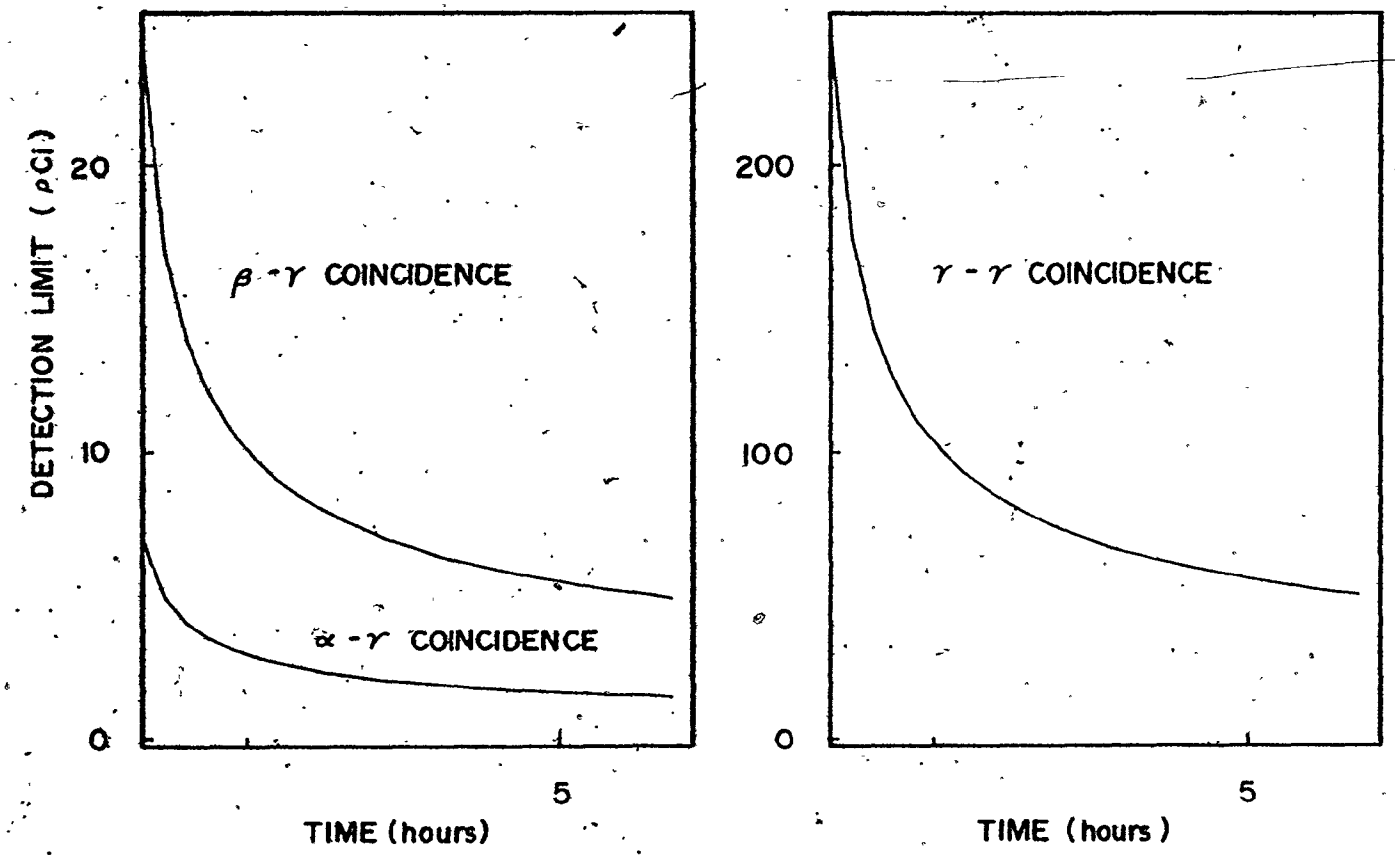

FIGURE 5.1 DETECTION LIMIT AS A FUNCTION OF TIME

CHAPTER 6

DATA ANALYSIS

6.1 Introduction

In order to determine the activity of ^{226}Ra, the sample counts per second must be either corrected for the efficiency of a particular counting system, or compared to a calibrated standard which was counted in an identical manner. The latter method was chosen for this work for one important reason: it was noted that the α and β plateaus of the proportional counter used in the α-γ /β-γ coincidence spectrometer were not well defined, and thus small changes in the high voltage supplied to the detector could easily affect the counts obtained during a measurement. By determining the ratio of sample counts per second to standard counts per second, the effect of high voltage fluctuations would tend to cancel out and better precision could be achieved; thus the standard was counted whenever a set of samples was counted.

The analysis procedure is discussed in the following sections.

6.2 α-γ Coincidence Spectra Analysis

The spectra from α-γ coincidence measurements were characterised by two peaks, the 0.186 MeV γ-ray peak from the alpha decay of ^{226}Ra to ^{222}Rn with the subsequent emission of a de-excitation -ray, and a radium X-ray peak located at 0.0885 MeV, as illustrated in figure 6.1, for the 10 pCi level and in figure 6.2 for the 1 nCi level. Spectra were integrated to determine the total count rate and the system background counting rate, accumulated over 70,000 seconds, was subtracted. These results were compared to the net count rate obtained from the standard.

6.3 β-γ Coincidence Spectra Analysis

6.3.1 Introduction

Typical β-γ coincidence spectra are shown in figure 6.3, and 6.4. The peaks appearing in these spectra were not all directly due to the ^{214}Bi, therefore integrating to find total counts per second would not represent the true activity of ^{214}Bi. Since the 0.609 MeV γ-ray peak is the most prominent peak from the decay of ^{214}Bi, and is well separated from other interfering peaks, it was chosen for the analysis. As can be seen in figures 6.3, and 6.4, the background on either side of this γ-ray peak is reasonably flat; thus it was decided to simply fit the background underneath the peak to either a straight line or a

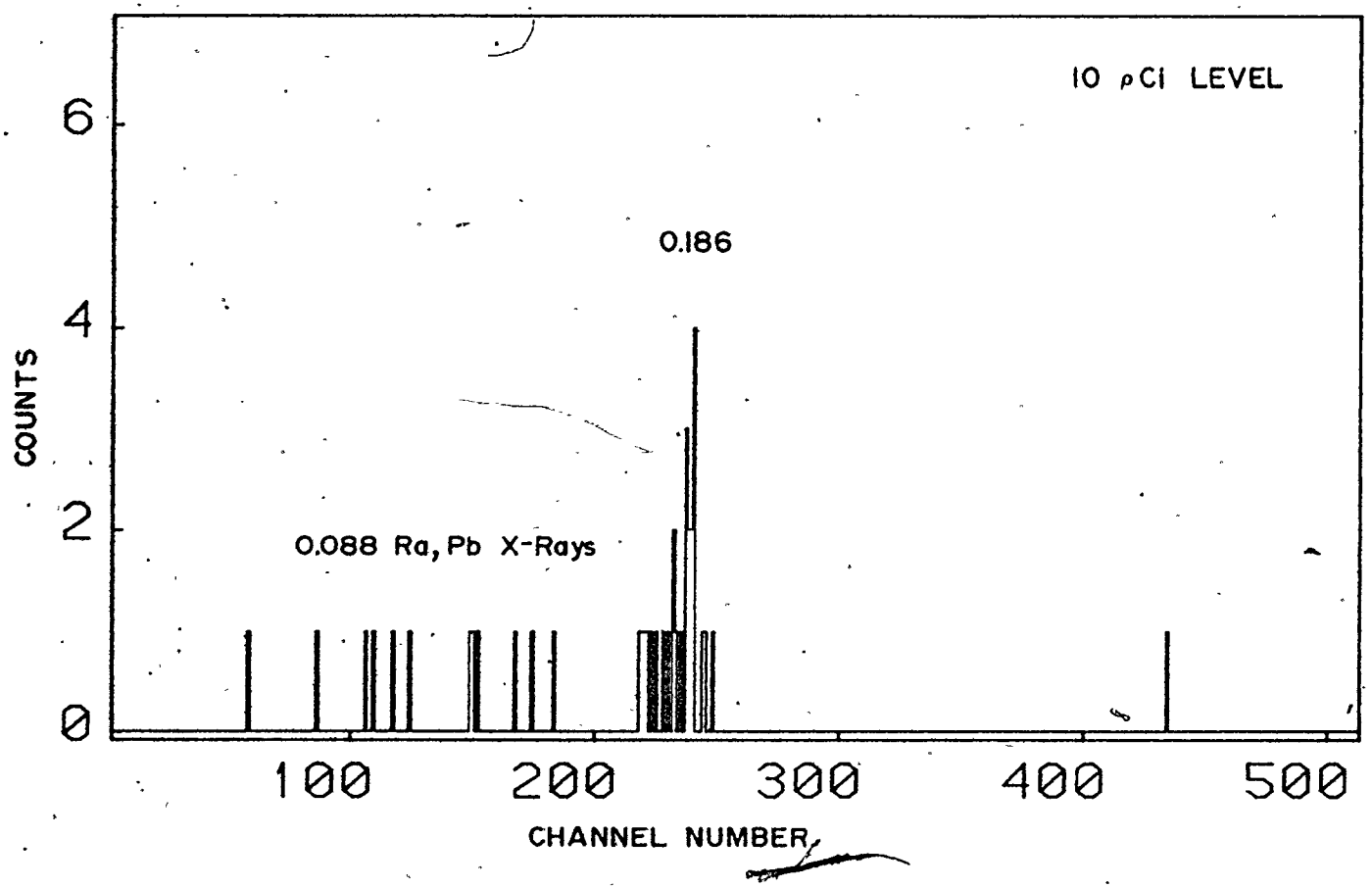

FIGURE 6.1 $\alpha - \gamma$ COINCIDENCE SPECTRUM (T = 4000 sec.)

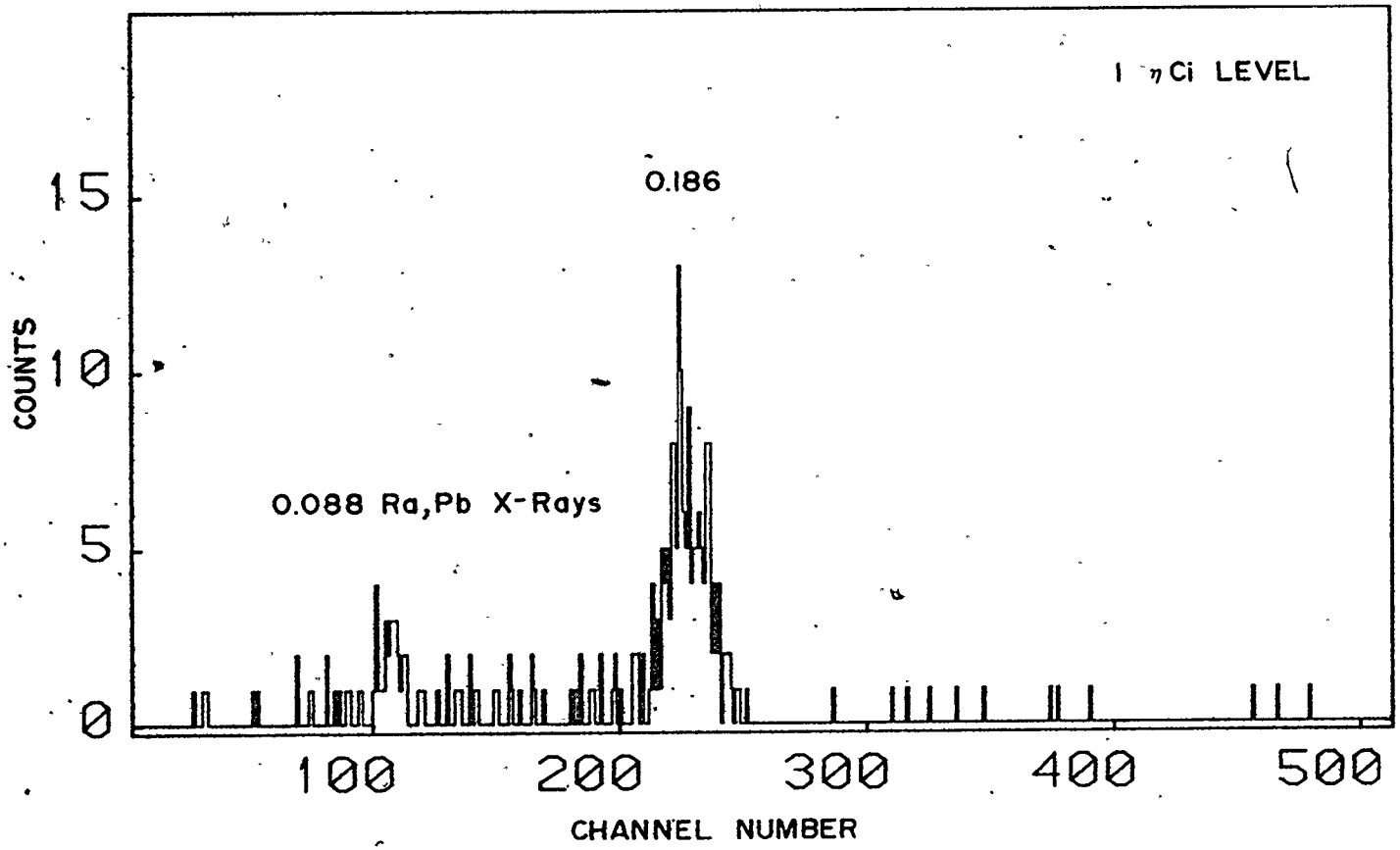

FIGURE 6.2 $\alpha-\gamma$ COINCIDENCE SPECTRUM (T=2000 sec)

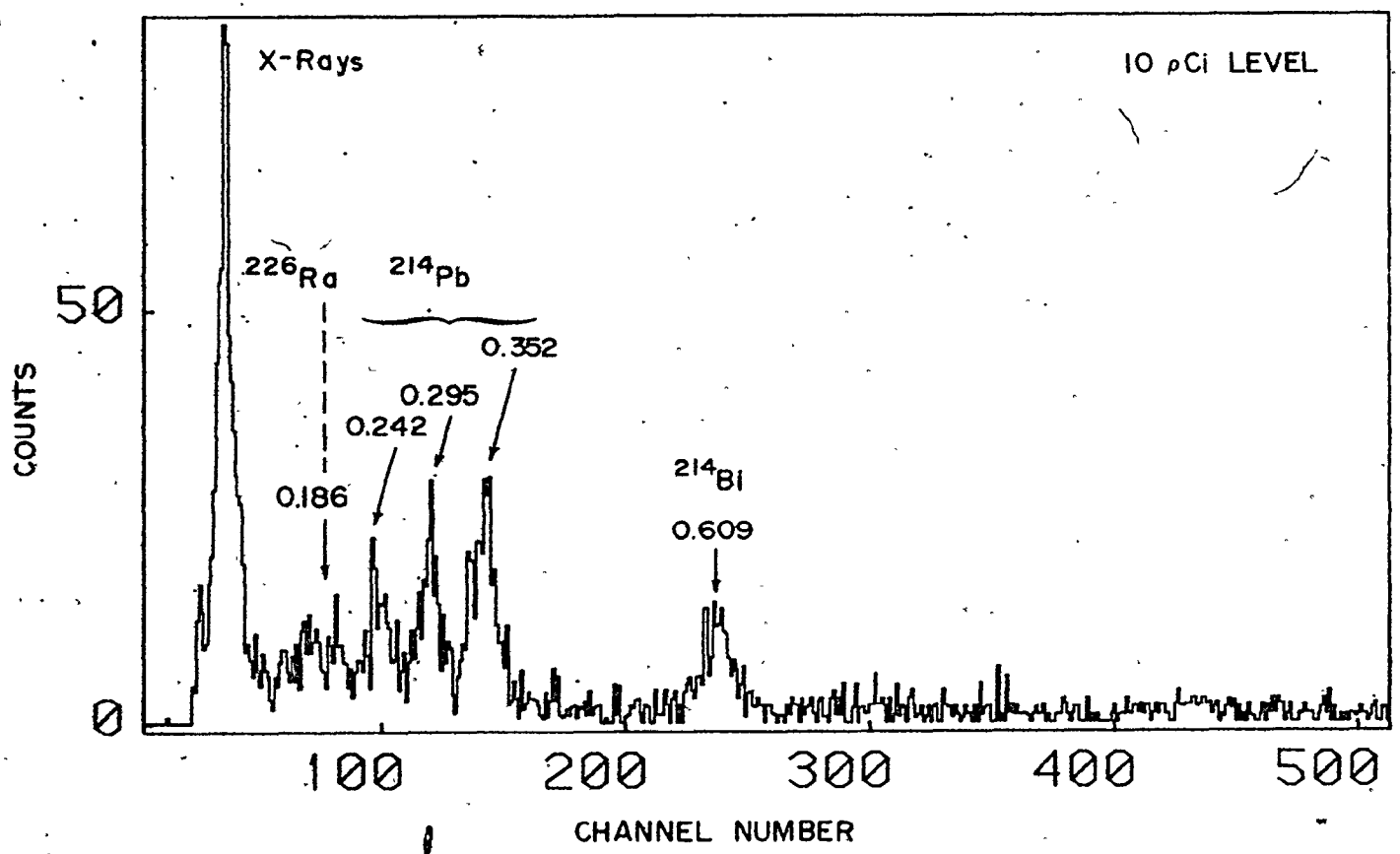

FIGURE 6.3 $\beta-\gamma$ COINCIDENCE SPECTRUM (T = 6000 sec)

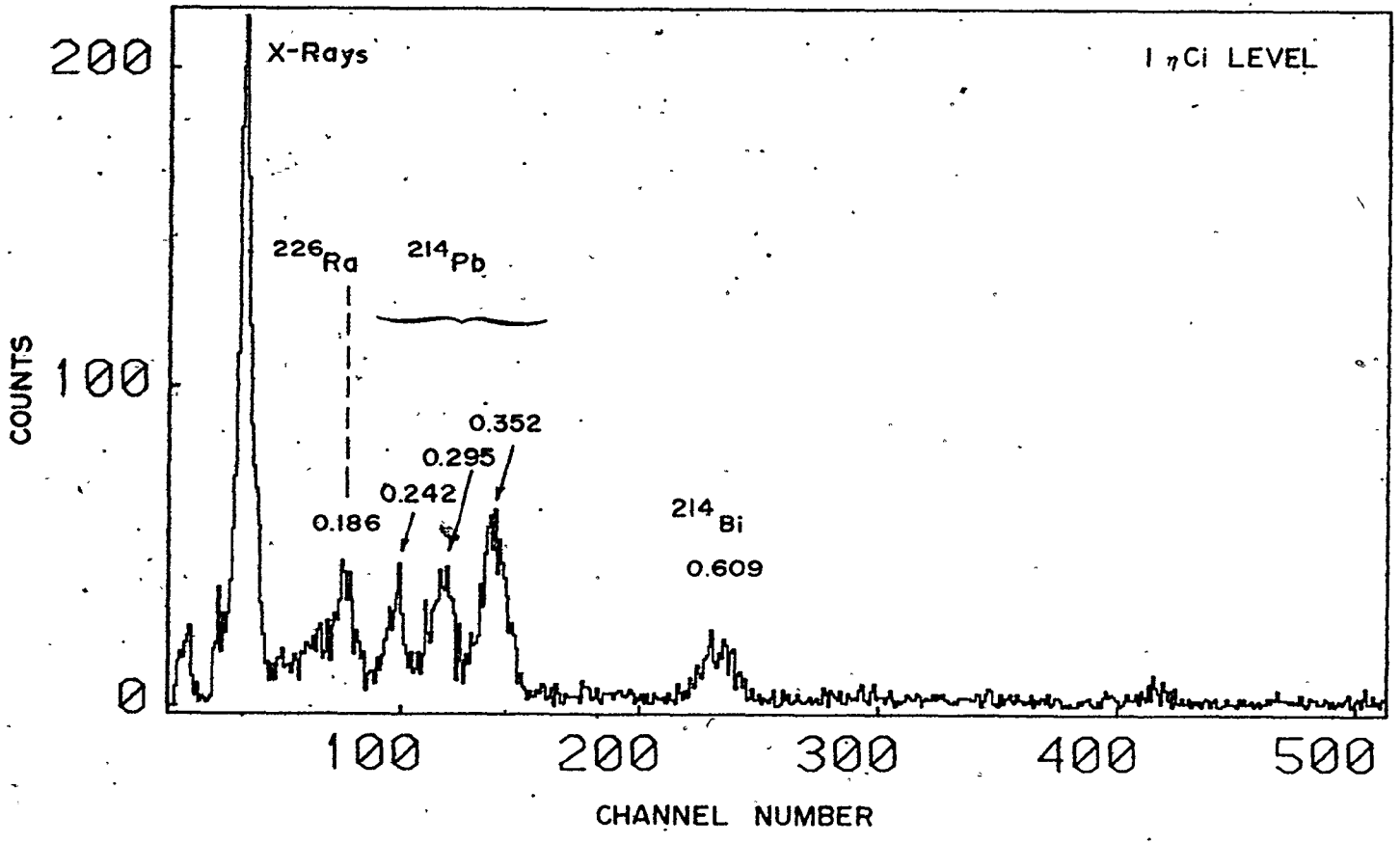

FIGURE 6.4 $\beta-\gamma$ COINCIDENCE SPECTRUM (T = 2000 sec)

quadratic.

One of the most popular methods for fitting background is the Method of Least Squares. A discussion of this method and the Method of Maximum Likelihood using Poisson Statistics, follows.

6.3.2 Methods of Maximum Likelihood and Least Squares

For data obtained from a counting experiment, the probability, P_i, for making the observed measurement, y_i, is given by the Poisson distribution, with mean $\mu_i = y(x_i)$:

$$P_i = \frac{[y(x_i)]^{y_i}}{y_i!} \cdot e^{-y(x_i)} \qquad 6.1$$

The probability for making an observed set of measurements of N values of y_i is given by the product of these individual probabilities:

$$\mathcal{L} = \prod_i P_i$$

$$= \prod_{i=1} \frac{[y(x_i)]^{y_i}}{y_i!} \cdot e^{-y(x_i)} \qquad 6.2$$

The Method of Maximum Likelihood may then be applied to this probability.

Consider the case where the fitting function is

linear;

$$y(x_i) = a + b.x_i, \text{ and then}$$

$$\mathcal{L}(a,b) = \prod_{i=1}^{N} \frac{(a + b.x_i)^{y_i} \cdot e^{-(a + b.x_i)}}{y_i!} \qquad 6.3$$

The Method of Maximum Likelihood consists of choosing, as estimates of the unknown parameters a and b, the particular values which maximize the Likelihood Function, $\mathcal{L}(a,b)$. However, $\ln[\mathcal{L}(a,b)]$ attains its maximum at the same values of a and b as $\mathcal{L}(a,b)$, and therefore it is easier to solve the Likelihood equations:

$$\frac{\partial \ln[\mathcal{L}(a,b)]}{\partial a} = 0 \text{ , and } \frac{\partial \ln[\mathcal{L}(a,b)]}{\partial b} = 0 \qquad 6.4$$

Then from equation 6.3:

$$\ln[\mathcal{L}(a,b)] = \sum [y_i \ln(a + b.x_i) - (a + b.x_i) - \ln y_i!] \qquad 6.5$$

$$\frac{\partial \ln[\mathcal{L}(a,b)]}{\partial a} = \sum_{i=1}^{N} \frac{y_i}{(a + b.x_i)} - N = 0$$

$$\frac{\partial \ln[\mathcal{L}(a,b)]}{\partial b} = \sum_{i=1}^{N} \frac{y_i . x_i}{(a + b.x_i)} - \sum_{i=1}^{N} x_i = 0$$

Rearranging, a pair of simultaneous equations which are not easily solved are obtained:

$$N = \sum \frac{y_i}{(a + b.x_i)} \qquad 6.6$$

$$\sum x_i = \sum \frac{y_i . x_i}{(a + b.x_i)} \qquad 6.7$$

However, to simplify the fitting procedure for data from counting experiments, it is usually assumed that the shapes of the individual Poisson distributions governing the fluctuations in the observed data, y_i, are nearly Gaussian(21).

On the basis of this assumption, the Likelihood Function becomes:

$$\mathcal{L}(a,b) = \prod_{i=1}^{N} \frac{1}{\sigma_i \sqrt{2\pi}} \exp \frac{-1}{2} \sum \frac{[y_i - y(x_i)]^2}{\sigma_i} \qquad 6.8$$

Since the first term in the above expression is a constant, independent of a and b, maximizing the probability $\mathcal{L}(a,b)$ is equivalent to minimizing the sum in the exponential. Therefore, the quantity x^2 may be defined as:

$$x^2 = \sum \frac{1}{\sigma_i^2} (y_i - a - b.x_i)^2 \qquad 6.9$$

This method for finding the best estimates of the

parameters a and b is termed the Method of Least Squares, because the optimum fit minimizes the weighted sums of squares of deviations, χ^2.

In order to determine these values of a and b we proceed as before and find:

$$\frac{\partial \chi^2}{\partial a} = 0, \quad \frac{\partial \chi^2}{\partial b} = 0$$

$$\sum \frac{y_i}{\sigma_i^2} = a \sum \frac{1}{\sigma_i^2} + b \sum \frac{x_i}{\sigma_i^2} , \qquad 6.10$$

$$\sum \frac{x_i \cdot y_i}{\sigma_i^2} = a \sum \frac{x_i}{\sigma_i^2} + b \sum \frac{x_i^2}{\sigma_i^2} \qquad 6.11$$

The solution of these equations can be found in one of several ways, as is discussed in many textbooks[22,23], and therefore will not be presented here. The Method of Least Squares can easily be extrapolated to higher order terms.

Problems can arise with this method, however, because the true weights, $1/\sigma_i^2$, of the data are never really known. Generally, the assumption is made that $\sigma_i^2 \simeq y_i$[21], and therefore the weighting for the data is $1/y_i$. If the count rates are low, it is possible for $y_i = 0$, which means special treatment or even exclusion of this data. It has been shown that a weight of $1/(y_i + 1)$ is a better

estimate of the true weight[24].

Proceeding with equations 6.3 and 6.5 instead of making the assumption that the observed fluctuations in the data y_i are governed by Gaussian statistics provides interesting results. Using an iterative procedure, estimates of the parameters a and b may be obtained without too much difficulty. A computer program, MLIKELY, was developed to fit the data with Poisson statistics, using the Method of Maximum Likelihood, for the present work. Initial guesses for the parameters a and b were entered into the program, as well as the desired increments. The value of the natural logarithm of the Likelihood Function, equation 6.5, was calculated, and the first parameter, a, was varied until the maximum value of equation 6.5 was attained. When this was completed, the second parameter, b, was varied until equation 6.5 again attained its maximum value. This entire procedure was then repeated until some criteria specifying the "goodness of fit" was reached. Once the parameters specifying the background were determined, the region underneath the γ-ray peak was integrated and subtracted from the total peak area to give net counts per second, which could then be related to the activity of ^{214}Bi. After making corrections for the ingrowth of ^{214}Bi, the activity of ^{226}Ra could be determined.

To find the variances, σ_a^2 and σ_b^2, and the

covariance, σ_{ab}^2, of the parameters, it could be assumed that the shape of the function $\ln[\mathscr{L}(a,b)]$, equation 6.5, around its maximum, is a parabola[21]. Then, from the Gaussian probability distribution, P(a,b), it is observed that:

$$\sigma_a^2 = -\frac{1}{\frac{\partial^2 \ln[P(a,b)]}{\partial a^2}}, \quad \sigma_b^2 = -\frac{1}{\frac{\partial^2 \ln[P(a,b)]}{\partial b^2}}$$

and $$\sigma_{ab}^2 = \frac{D}{1 + D}\ \sigma_a^2 \cdot \sigma_b^2 ,$$

$$D = \frac{\partial^2 \ln[P(a,b)]}{\partial a \partial b} .$$

If these results are then applied to the present case where fluctuations in the observed data, y_i, are governed by Poisson statistics, from equation 6.5 it is found that:

$$-\frac{\partial^2 \ln[\mathscr{L}(a,b)]}{\partial a^2} = \frac{y_i}{(a + b.x_i)^2}, \qquad 6.12$$

$$-\frac{\partial^2 \ln[\mathscr{L}(a,b)]}{\partial b^2} = \frac{y_i . x_i^2}{(a + b.x_i)^2}, \qquad 6.13$$

$$-\frac{\partial^2 \ln[\mathcal{L}(a,b)]}{\partial a \partial b} = \sum \frac{y_i . x_i}{(a + b.x_i)^2}, \quad 6.14.$$

Therefore, from equations 6.12, 6.13, and 6.14;

$$\sigma_a^2 = \frac{1}{\sum \frac{y_i}{(a + b.x_i)^2}}$$

$$\sigma_b^2 = \frac{1}{\sum \frac{y_i . x_i^2}{(a + b.x_i)^2}}$$

$$\sigma_{ab}^2 = \frac{\sum \frac{y_i . x_i}{(a + b.x_i)^2}}{1 - \sum \frac{y_i . x_i}{(a + b.x_i)^2}} . \sigma_a^2 . \sigma_b^2 .$$

A comparison was made between the Method of Maximum Likelihood, using Poisson statistics, and the method of Least Squares, to see which technique gave the best fit to sets of test data. In order to do this comparison, six test files were created. For each set of data a gaussian peak, specified by the full width at half the maximum height, (FWHM), and the total peak area with statistics, was generated. Background noise with a Poisson distribution was then added to each peak. The FWHM and peak area were chosen

such that the test data would be similar to the actual experimental data. The test files were then fitted in five ways:

1) the Method of Maximum Likelihood, using Poisson statistics - linear fit to the background,
2) the Method of Least Squares;
   i) linear fit with weight = $1/y_i$ and channels with zero counts assigned a weight of one,
   ii) linear fit with weight = $1/(y_i+1)$,
   iii) quadratic fit with weight = $1/y_i$ and channels with zero counts assigned a weight of one,
   iv) quadratic fit with weight = $1/(y_i+1)$.

Results of these fits are shown in tables 6.1, 6.2, and 6.3, where various peak widths were chosen. Column 2 represents the real peak area, column 3 shows the peak area calculated using method 1), as described above, column 4 shows the peak area calculated using method 2)-iii), column 5 using method 2)-iv), column 6 using method 2)-i), and finally, column 7 shows the peak area calculated using

TABLE 6.1

ANALYSIS OF SIMULATED TEST DATA : NARROW PEAK

FWHM	A_{REAL}	$A_{MAX.L.}$	$A^{Q}_{L.S.}(0)$	$A^{Q}_{L.S.}(1)$	$A^{L}_{L.S.}(0)$	$A^{L}_{L.S.}(1)$
5	22	24 ±6	22 ±7	23 ±7	26 ±6	25 ±0
47-63*	20	21 ±6	16 ±7	17 ±7	23 ±6	22 ±9
7	13	13 ±5	10 ±6	11 ±6	15 ±5	14 ±8
47-63	22	26 ±6	20 ±7	21 ±7	28 ±6	27 ±10
9	21	22 ±6	18 ±7	19 ±7	23 ±6	23 ±9
47-63	16	16 ±6	11 ±6	12 ±6	18 ±5	17 ±9
VARIANCE		22	58	39	67	48

* 47-63 represents the channel numbers designating the peak position.

TABLE 6.2

ANALYSIS OF SIMULATED TEST DATA : MEDIUM PEAK

FWHM	A_{REAL}	$A_{MAX.L.}$	$A^{Q}_{L.S.}(0)$	$A^{Q}_{L.S.}(1)$	$A^{L}_{L.S.}(0)$	$A^{L}_{L.S.}(1)$
5	22	24 ±7	22 ±8	23 ±8	27 ±6	26 ±10
45-65*	20	23 ±6	18 ±7	18 ±7	25 ±6	24 ±10
7	13	12 ±6	8 ±7	10 ±7	14 ±5	13 ±8
45-65	22	25 ±7	18 ±8	19 ±8	27 ±6	27 ±10
9	21	20 ±6	14 ±8	16 ±8	21 ±6	21 ±10
45-65	16	16 ±6	10 ±7	11 ±7	19 ±6	18 ±10
VARIANCE		27	130	.74	85	58

* 45-65 represents the channel numbers designating the peak position.

TABLE 6.3

ANALYSIS OF SIMULATED TEST DATA : WIDE PEAK

FWHM	A_{REAL}	$A_{MAX.L.}$	$A^{Q}_{L.S.}(0)$	$A^{Q}_{L.S.}(1)$	$A^{L}_{L.S.}(0)$	$A^{L}_{L.S.}(1)$
5	22	22 ±7	18 ±9	20 ±9	25 ±7	24 ±11
42-68*	20	24 ±7	18 ±8	18 ±8	27 ±7	26 ±11
7	13	8 ±6	3 ±9	5 ±9	11 ±5	10 ±9
42-68	22	29 ±7	19 ±8	20 ±8	32 ±7	31 ±11
9	21	19 ±7	12 ±9	14 ±9	21 ±6	20 ±10
42-68	16	16 ±4	8 ±8	9 ±8	19 ±6	18 ±10
VARIANCE		95	271	174	163	131

* 42-68 represents the channel numbers designating the peak position.

method 2)-ii). The last row in each table represents the sum of the squares of the deviations of the fitted area to the real area, for each method of fitting. It is clearly shown that the Method of Maximum Likelihood gave the best results, for all three peak regions. The linear least squares fit with weight = $1/(y_i+1)$ gave the next best fit in two of the three cases. These results also show that all five methods for fitting the test files were sensitive to the peak region chosen, and thus care must be taken when choosing this region for the experimental data.

As a result of this comparison, peak areas for all the experimental data were obtained using the Method of Maximum Likelihood.

6.4 γ-γ Coincidence Spectra Analysis

With the coincidence circuit set up as described in section 3.3.3, the 0.609 MeV γ-ray peak from ^{214}Bi was the only peak which appeared in the γ-γ coincidence specta, as shown in figures 6.5, and 6.6. However, unlike the α-γ coincidence spectra, many scattered events contributed to the total counts appearing in the spectra. These events resulted from the many γ-rays in coincidence with the 0.609 MeV γ-ray. It was thus necessary to determine this background component of the peak using fitting techniques. The γ-γ coincidence data were fitted in a similar manner to

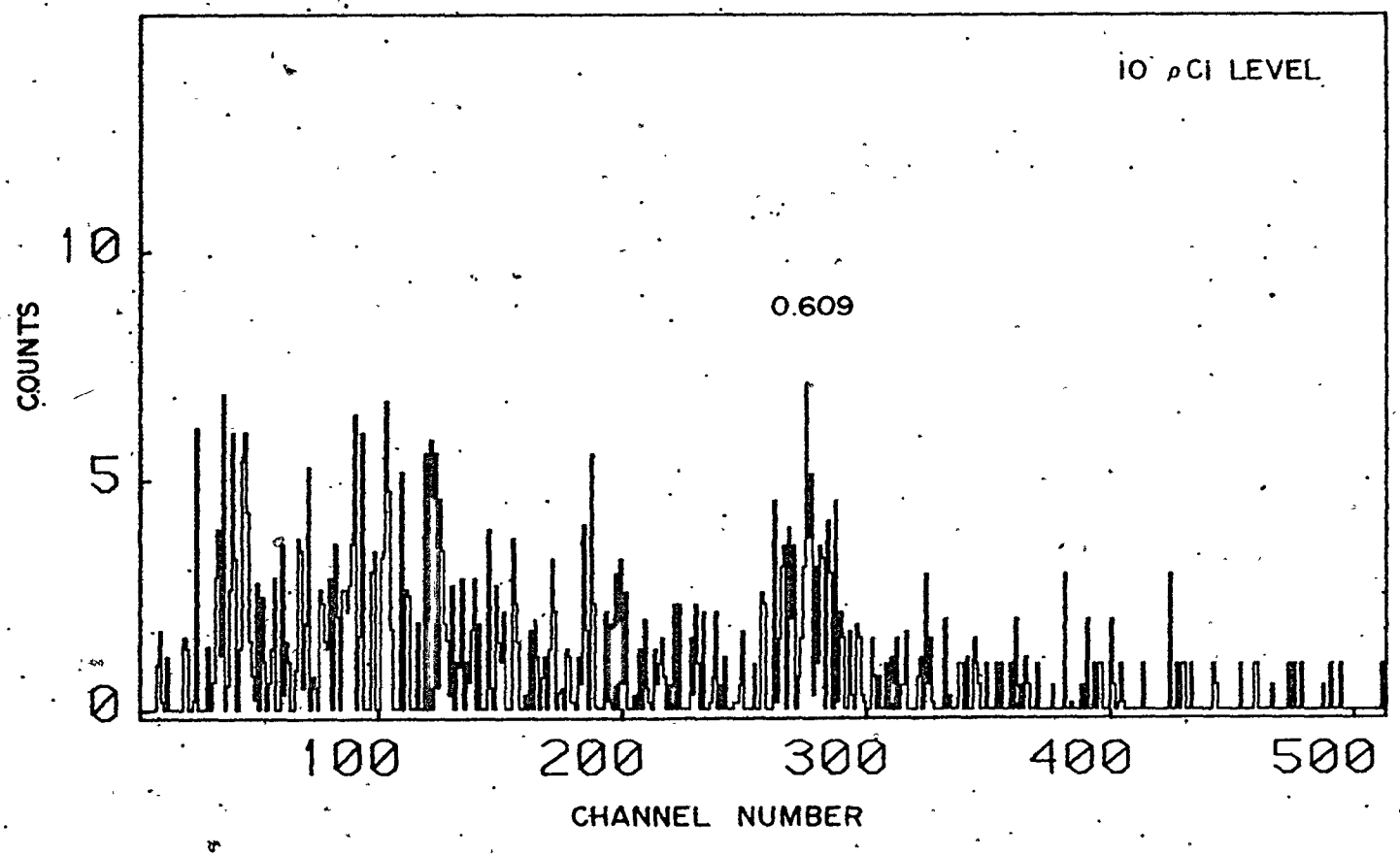

FIGURE 6.5 $\gamma-\gamma$ COINCIDENCE SPECTRUM (T= 30,000 sec)

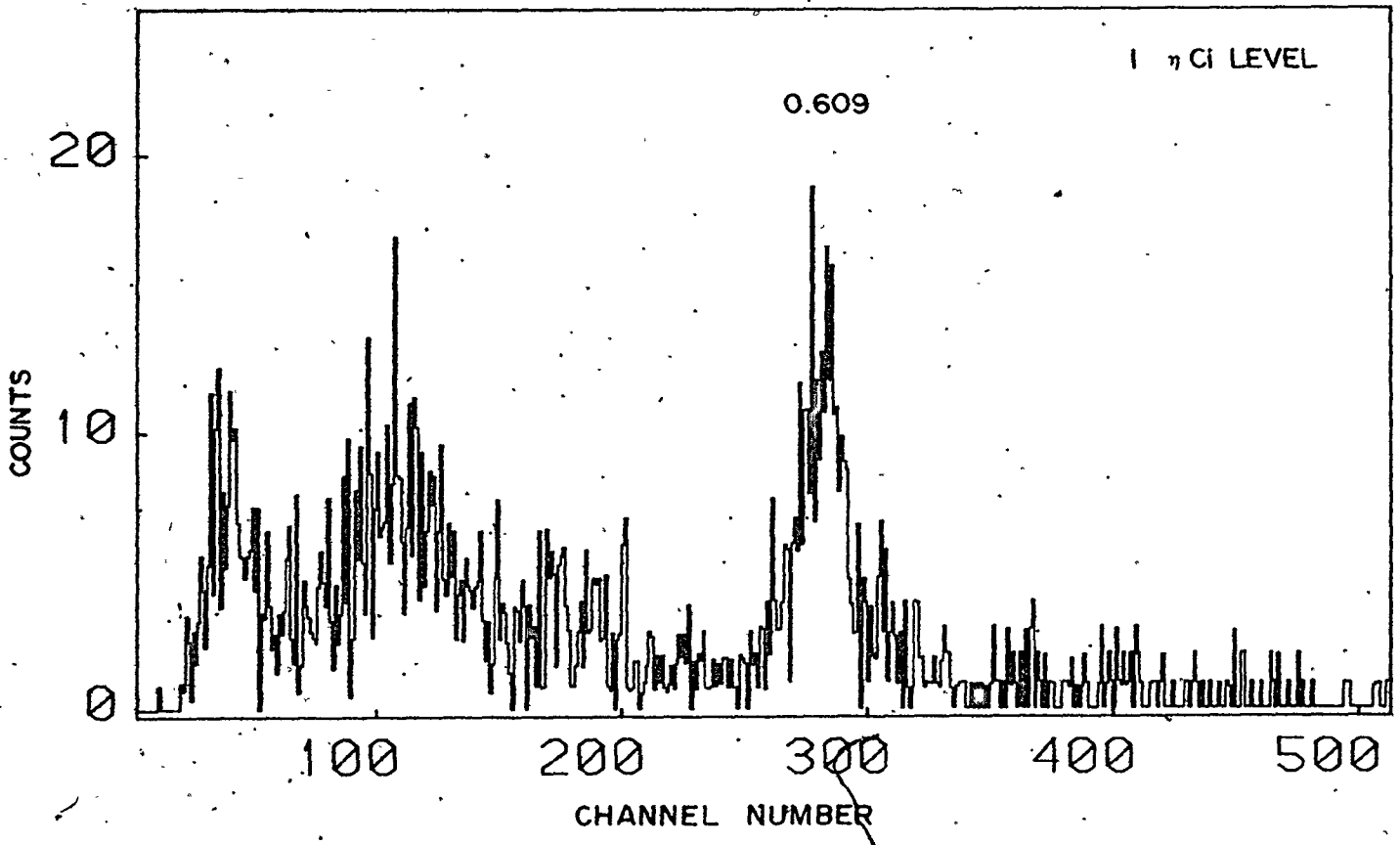

FIGURE 6.6 $\gamma - \gamma$ COINCIDENCE SPECTRUM (T = 5000 sec)

the β-γ coincidence data, using the Method of Maximum Likelihood with Poisson statistics.

6.5 Standard Calibration

A standard was prepared from a stock solution containing approximately 1 nCi per ml of ^{226}Ra, as described in chapter 4. Owing to the relatively low activity, calibration required counting the sample directly on the face of a 7.5 cm by 7.5 cm NaI(Tl) detector, rather than in a standard geometry a few centimeters away. Counting in this geometry could present summing problems in the γ-ray peak of interest, the 0.609 MeV γ-ray peak. Therefore, to obtain the sample count rate, the area under the four lower energy peaks appearing in the singles spectrum, figure 6.7, was determined, using the Method of Maximum Likelihood, as discussed in section 6.3.2. A 0.0993 ± 10% μCi ^{226}Ra standard was counted in the same geometry and analysed in the same manner as above, in order to obtain the actual activity of the ^{226}Ra-$BaSO_4$ precipitate standard.

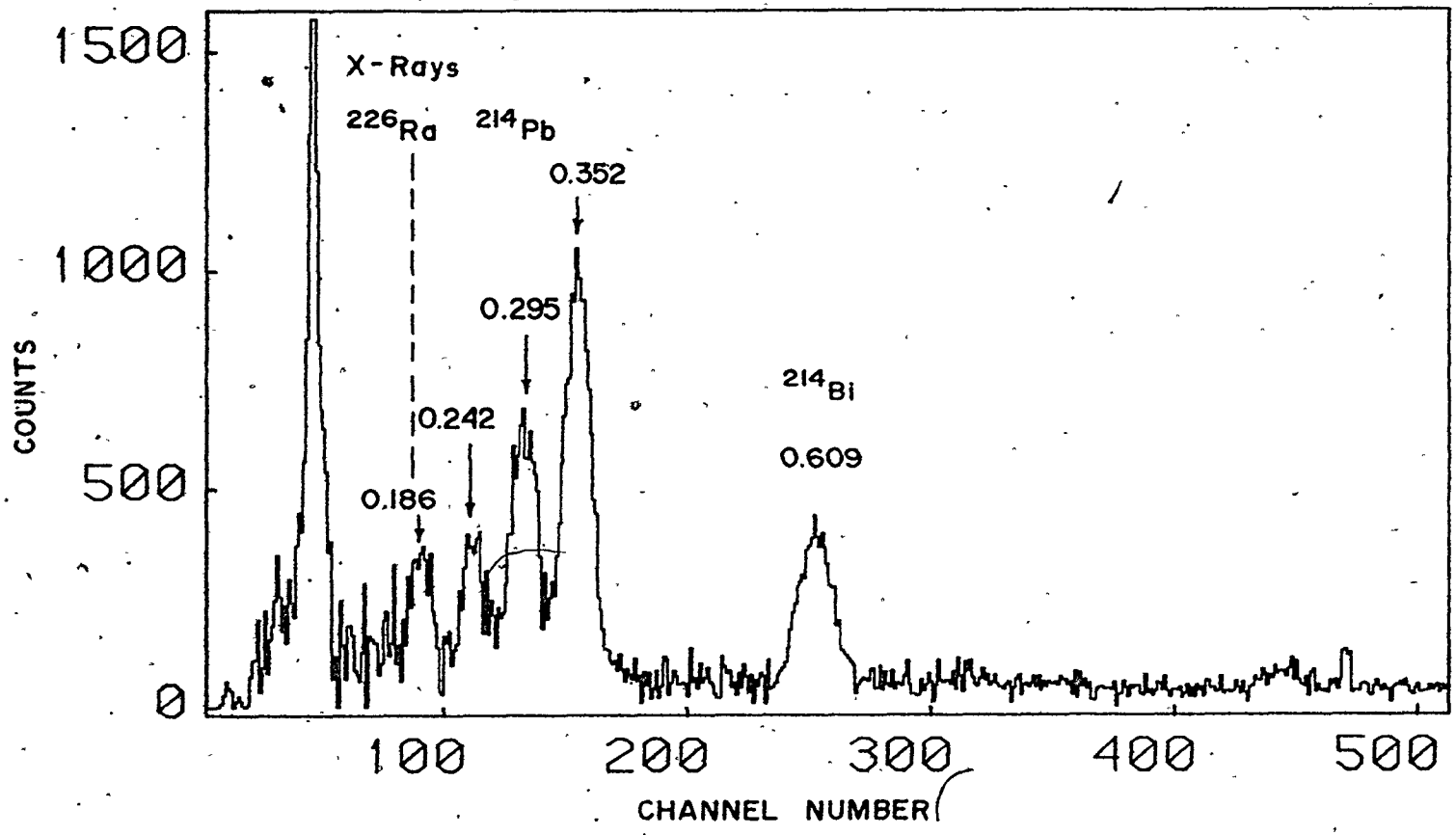

FIGURE 6.7 γ SINGLES SPECTRUM, STANDARD (T = 4000 sec)

CHAPTER 7

EXPERIMENTAL RESULTS

7.1 Standard Calibration

The ^{226}Ra standard was calibrated as described in section 4.5. The results of three measurements are shown in table 7.1. The weighted mean of the three trials was calculated to be 1.2 ± 0.1 nCi. Therefore, this standard activity was used to calibrate the absolute activities for the results in the following manner:

$$\text{Activity} = \frac{\text{sample cts/sec}}{\text{standard cts/sec}} \quad 1.2 \pm 0.1 \text{ nCi}$$

7.2 1 nCi Level Results

Two samples were prepared, according to section 5.2, from a radium stock solution containing approximately 1 nCi/ml of ^{226}Ra. The first sample was precipitated with 0.5 mg of Ba^{+2} as carrier, and the second with 1.0 mg Ba^{+2}. Results of α-γ and β-γ coincidence measurements for several trials are presented in tables 7.2 and 7.3. In these tables, the activities in nCi for samples counted for a period of 2000 seconds, are shown. The β-γ coincidence results have been corrected for the ingrowth of ^{214}Bi.

The standard deviation and coefficient of variation

TABLE 7.1

STANDARD CALIBRATION RESULTS

TRIAL	ACTIVITY (ηCi)
1	1.4 ± 0.1
2	1.0 ± 0.1
3	1.6 ± 0.2
WEIGHTED MEAN	1.21 ± 0.1

TABLE 7.2

α-γ COINCIDENCE RESULTS : 1 nCi LEVEL

TRIAL	SAMPLE THICKNESS	
	0.5 mg	1.0 mg
1	1.3 ± 0.1	1.6 ± 0.1
2	1.5 ± 0.1	1.4 ± 0.1
3	1.4 ± 0.1	1.3 ± 0.1
4	1.2 ± 0.1	1.3 ± 0.1
5	1.2 ± 0.1	1.3 ± 0.1
6	1.2 ± 0.1	1.3 ± 0.1
7	1.4 ± 0.1	1.5 ± 0.1
8	1.3 ± 0.1	1.4 ± 0.1
9	1.2 ± 0.1	1.4 ± 0.1

TABLE 7.3

β-γ COINCIDENCE RESULTS : 1 nCi LEVEL

TRIAL	SAMPLE THICKNESS	
	0.5 mg	1.0 mg
1	0.91 ± 0.06	1.04 ± 0.06
2	0.99 ± 0.06	0.96 ± 0.06
3	0.95 ± 0.06	1.06 ± 0.06
4	0.90 ± 0.06	1.18 ± 0.07
5	1.01 ± 0.09	1.04 ± 0.09
6	1.02 ± 0.09	1.3 ± 0.1
7	1.1 ± 0.1	1.07 ± 0.09
8	1.1 ± 0.1	1.2 ± 0.1
9	----	1.1 ± 0.1

were calculated using the following expressions:

$$S = \sqrt{\frac{(\bar{n}-n)^2}{N-1}} \quad \text{and} \quad V = \frac{S}{\bar{n}} \cdot 100 \ ,$$

where: n = observed activity,

$\bar{n}$ = mean of observed activity,

N = number of trials.

These results are shown in table 7.4.

From table 7.4, the activities calculated for the 0.5 mg and 1.0 mg samples were 1.3 nCi and 1.4 nCi, respectively, for the α-γ method, and 1.0 nCi and 1.1 nCi for the β-γ method. The reults for the two sample thicknesses agreed within error; thus the sample thickness had no apparent effect. However, the α-γ coincidence measurements resulted in slightly higher activities for both of the samples, than did the β-γ coincidence measurements.

TABLE 7.4

PRECISION MEASUREMENTS : 1 ηCi LEVEL

SAMPLE THICKNESS		α-γ	β-γ
0.5 mg	AVERAGE	1.3 ηCi	1.0 ηCi
	S	0.2	0.1
	V	12%	8%
1.0 mg	AVERAGE	1.4 ηCi	1.1 ηCi
	S	0.1	0.1
	V	8%	9%

7.3 10 pCi Level Results

Seven samples were prepared from a radium stock solution containing approximately 10 pCi/ml. of ^{226}Ra. Five of these samples were precipitated with 0.5 mg Ba^{+2} as carrier, and the remaining two samples contained 1.5 mg and 3.5 mg Ba^{+2}, respectively. Results of α-γ, β-γ, and γ-γ coincidence measurements for several trials are shown in tables 7.5, 7.6, and 7.7. Sample counts were collected for periods of 4000 and 30,000 seconds for the α-γ and γ-γ coincidence measurements, respectively, whereas counting periods of 4000 and 6000 seconds were used for the β-γ coincidence measurements. The β-γ and γ-γ coincidence results were corrected for the ingrowth of ^{214}Bi.

The standard deviation and coefficient of variation were calculated using the expressions given previously. These results are shown in table 7.8.

It is evident from these results that sample thicknesses in the range 0.5 mg Ba+2 to 3.5 mg Ba+2 have no effect on the activities measured. For example, from the α-γ coincidence results in table 7.8, the average activity for sample #1, prepared with 0.5 mg Ba^{+2}, was 17 pCi with a standard deviation of 8 pCi, whereas for a 1.5 mg Ba^{+2} sample, #6, the average activity and standard deviation were 12 pCi and 3 pCi, respectively. These results agreed within error. The average activity calculated for sample #1 from

TABLE 7.5

α-γ COINCIDENCE : 10 pCi LEVEL

SAMPLE (Thickness in mg)						
1	2	3	4	5	6	7
0.5	0.5	0.5	0.5	0.5	1.5	3.5
16 ±6	23 ±7	76 ±14	7 ±4	18 ±6	13 ±5	37 ±9
25 ±8	31 ±8	62 ±12	21 ±7	24 ±7	11 ±5	42 ±10
8 ±4	22 ±7	77 ±14	6 ±4	26 ±8	12 ±5	56 ±12
24 ±8	22 ±7	93 ±16	12 ±5	16±6	10 ±5	33 ±9
11 ±5	22 ±7	80 ±15	18 ±6	12 ±5	18 ±6	20 ±7
17 ±6	19 ±7	71 ±14	20 ±7	10 ±5	9 ±5	54 ±11
26 ±7	17 ±6	63 ±12	17 ±6	17 ±6	8 ±4	35 ±9
6 ±4	9 ±4	59 ±12	23 ±7	------	10 ±5	32 ±8
21 ±7	28 ±8	74 ±13	10 ±5	------	15 ±6	47 ±10
------	------	------	19 ±6	------	15 ±6	------

TABLE 7.6

β-γ COINCIDENCE : 10 pCi LEVEL

SAMPLE (Thickness in mg)						
1	2	3	4	5	6	7
0.5	0.5	0.5	0.5	0.5	1.5	3.5
23 ±5	8 ±3	63 ±10	24 ±5	15 ±4	16 ±4	63 ±9
25 ±6	17 ±5	49 ±9	12 ±4	18 ±4	14 ±4	31 ±6
20 ±5	16 ±5	84 ±10	26 ±5	17 ±5	21 ±5	46 ±8
8 ±4	20 ±5	70 ±8	21 ±4	12 ±3	14 ±3	30 ±5
12 ±4	25 ±5	88 ±9	19 ±4	18 ±4	9 ±3	29 ±4
10 ±3	18 ±4	52 ±6	21 ±4	12 ±3	11 ±3	50 ±6
9 ±3	28 ±4	67 ±8	20 ±4	12 ±3	8 ±2	45 ±6
18 ±4	18 ±4	73 ±9	12 ±3	14 ±3	8 ±3	50 ±6
10 ±3	21 ±4	70 ±9	12 ±4	22 ±4	11 ±3	46 ±6
18 ±4	20 ±4	57 ±9	6 ±3	14 ±4	7 ±3	44 ±4
------	------	------	9 ±4	------	10 ±3	46 ±7

TABLE 7.7

γ-γ COINCIDENCE RESULTS : 10 pCi LEVEL

SAMPLE	TRIAL 1	TRIAL 2
1	28 ± 9	-------
2	11 ± 7	-------
3	96 ± 15	41 ± 10
4	19 ± 9	12 ± 7
5	18 ± 9	10 ± 8
6	14 ± 6	11 ± 7
7	39 ± 10	-------

TABLE 7.8

PRECISION MEASUREMENTS : 10 pCi LEVEL

SAMPLE		α-γ	β-γ	γ-γ
1	AVERAGE	17	15	---
0.5 mg	S	6	6	---
	V	44%	39%	---
2	AVERAGE	21	19	---
0.5 mg	S	6	5	---
	V	29%	28%	---
3	AVERAGE	73	62	69
0.5 mg	S	11	13	39
	V	15%	19%	56%
4	AVERAGE	15	16	16
0.5 mg	S	6	7	5
	V	40%	41%	32%
5	AVERAGE	18	15	14
0.5 mg	S	6	3	5
	V	33%	21%	37%
6	AVERAGE	12	12	6
1.5 mg	S	3	4	7
	V	26%	37%	110%
7	AVERAGE	40	44	---
3.5 mg	S	11	10	---
	V	27%	23%	---

the β-γ coincidence results was 15 pCi with a standard deviation of 6 pCi. This result compares favourably to the result given above for the α-γ coincidence technique. Thus, as seen in table 7.8, the average activities calculated for the α-γ and β-γ coincidence measurements agreed within error, as did the coefficient of variation averaged over the seven samples.

The standard deviation and coefficient of variation for the γ-γ coincidence measurements were found to be much higher than for the α-γ and β-γ measurements, ($V(\gamma-\gamma)$ = 56.2% as compared to $V(\alpha-\gamma)$ = 14.6% for sample #3). However, these parameters were calculated on the basis of only two measurements; thus the results are inconclusive. Nevertheless, the average activities calculated agreed with the α-γ and β-γ results.

7.4 Uranium Mill Sample

Finally, a uranium tailings water sample received from the International Nickel Corporation, (INCO), was analysed. Spectra from the α-γ and β-γ coincidence measurements are shown in figures 7.1 and 7.2. The activities were calculated to be 6 $\pm$1 and 13 $\pm$ 2 pCi. for the α-γ, and β-γ results, respectively. It is apparent from the α-γ measurement that some ^{223}Ra was present in the sample at the time that it was counted. The 0.149, 0.270,

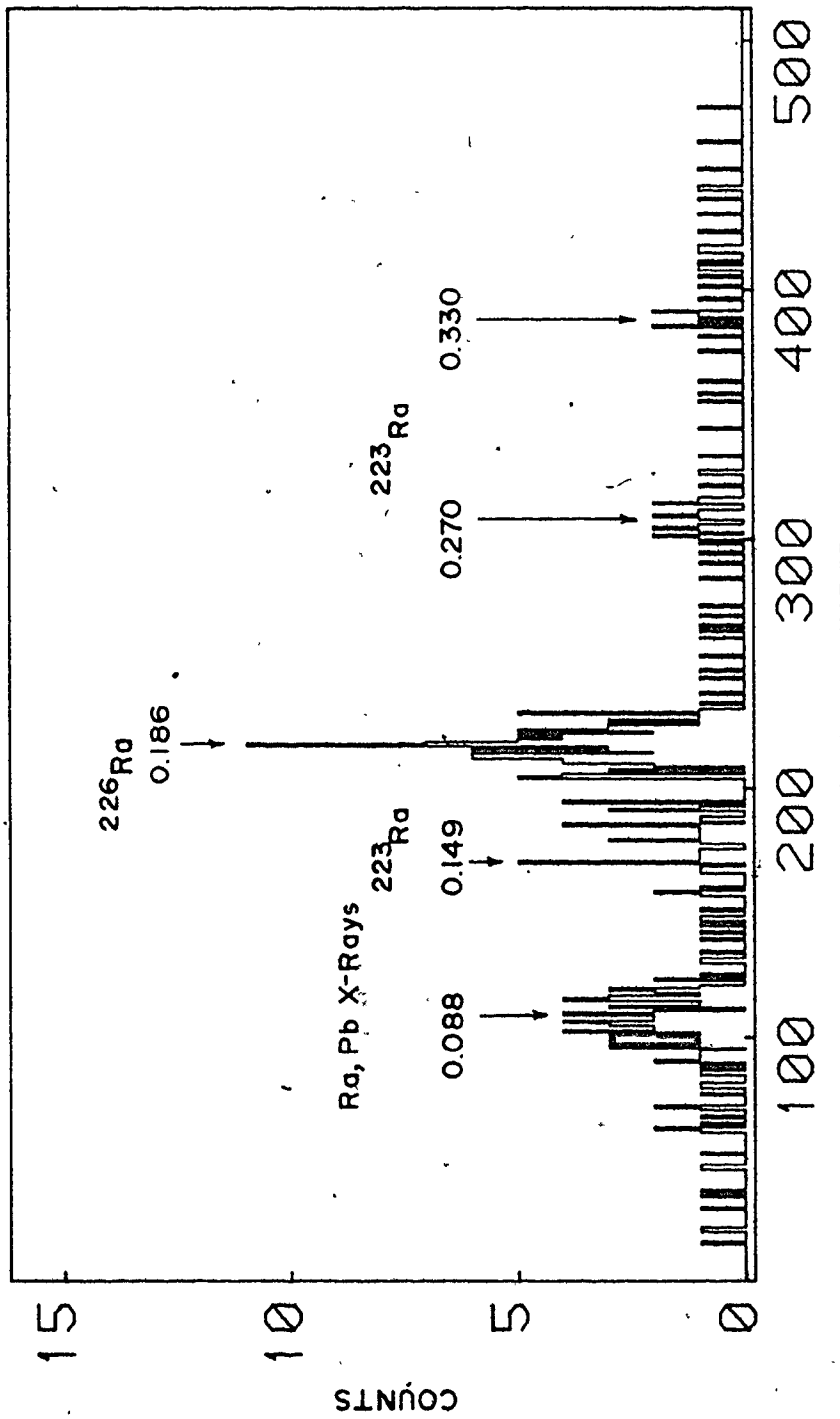

FIGURE 7.1 $\alpha-\gamma$ COINCIDENCE SPECTRUM, URANIUM MILL SAMPLE

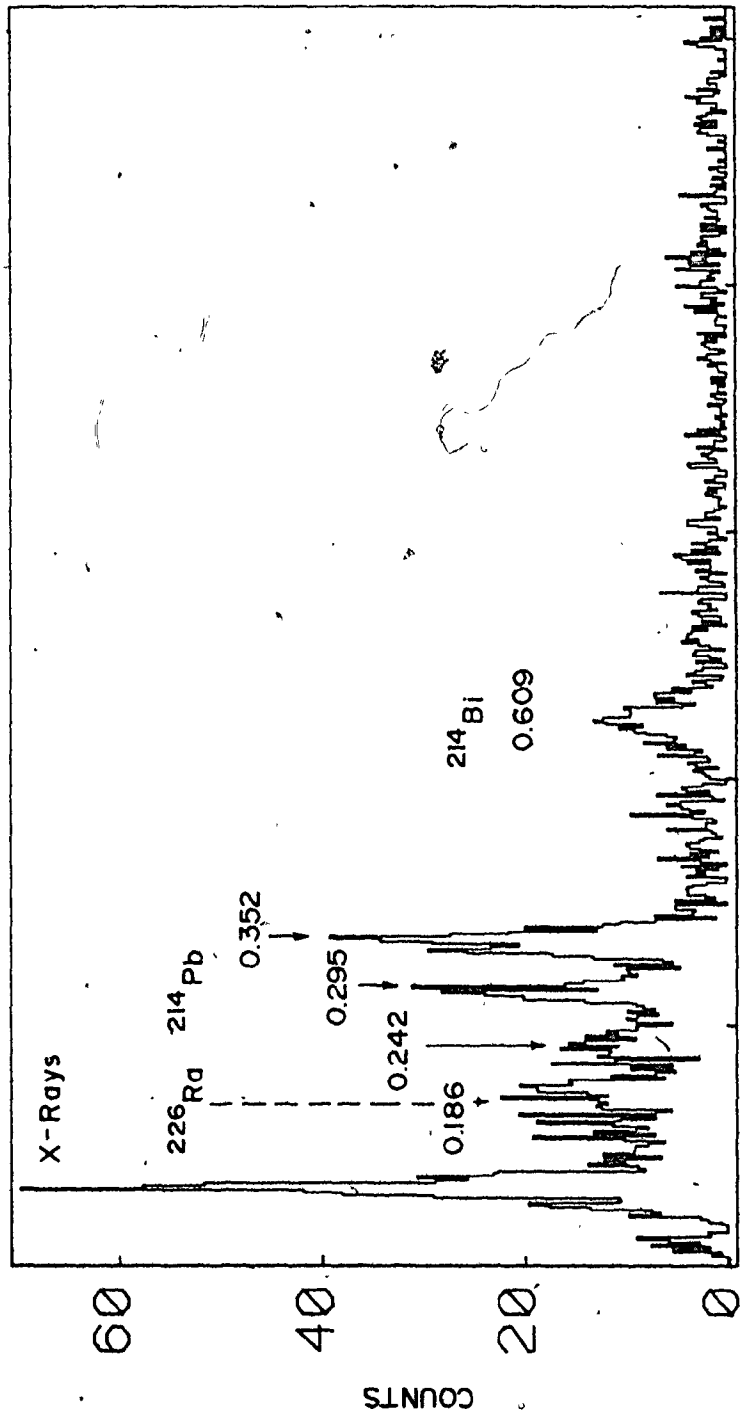

FIGURE 7.2 $\beta-\gamma$ COINCIDENCE SPECTRUM, URANIUM MILL SAMPLE

and 0.330 MeV. γ-ray peaks associated with the decay of ^{223}Ra to ^{219}Rn are identified in figure 7.1. If the ^{223}Ra contribution to the spectrum had been significant, the total counts measured would have had to be corrected for this activity. Additional analysis such as this should not present any problems, since the 0.186 MeV. γ-ray peak from the decay of ^{226}Ra is separated from the interfering γ-ray peaks. The half-lives of the ^{223}Ra daughter products are very short; therefore ^{223}Ra was not detected in the β-γ measurements, since this data was collected a few days after the α-γ coincidence data.

The activity determined from an alpha spectrometric measurement was 8 pCi. This is in close agreement to the results given in the present work.

7.5 Discussion

The results presented here indicate that of the three coincidence techniques investigated, the α-γ technique is the most attractive on the basis of detection limit and simplicity of data analysis. The γ-γ coincidence technique is the least sensitive, and thus would not be recommended for the analysis of ^{226}Ra concentrations in water. This result was not unexpected, since this system was originally developed for the purpose of analysing radium in soil samples.

The agreement between the three techniques is quite good, as indicated in tables 7.4 and 7.8. At the 1 nCi level, the α-γ coincidence measurements resulted in slightly higher activities for the two samples than the β-γ coincidence measurements. However, the 10 pCi level results indicated no difference in activities between the two systems over a series of seven samples. It was thus concluded that the results of both the α-γ and β-γ coincidence measurements were in close agreement.

CHAPTER 8

CONCLUSIONS

8.1 Comparison With Existing Methods

At first sight, the coefficient of variation for the coincidence techniques seems quite high compared to other techniques for measuring ^{226}Ra in water. J.B. Zimmerman[18] found that using an alpha spectrometric technique, as previously described in section 1.2, the coefficient of variation for the procedure at the 5 pCi level was 11.4% for a counting time of 2000 seconds. Employing the radon emanation technique, E. Pohl[8] determined that an error of ± 20% for a radon content of 1 pCi within a 20 liter chamber could be achieved. This corresponds to 0.05 pCi/liter of ^{222}Rn in the air. It must be remembered, however, that in the present work samples were counted for periods of time corresponding to the detection limit, as discussed in chapter 6. By increasing, but still maintaining a reasonable counting time, improved counting statistics and thus improved precision could be achieved.

Despite the lower precision, the present coincidence counting techniques have certain desirable features over other methods. Compared to the radon emanation technique, the total sample preparation and counting time is reduced by several days. This alone could be a deciding factor when considering a routine analysis procedure for ^{226}Ra.

The alpha spectrometric technique was briefly described in section 1.2. Samples are prepared in a similar manner as for the present work; ^{226}Ra is co-precipitated with barium sulphate onto filter discs. The samples are then counted on a silicon surface barrier detector which operates at a high voltage of approximately -185 volts. Since surface barrier detectors are sensitive to the ambient atmosphere the counting chamber must be evacuated. Samples are generally counted at a source detector distance of 10 mm. The electronic system consists of a preamplifier, amplifier and multichannel analyser. A typical count rate for a ^{226}Ra precipitate sample would be approximately 4 counts/sec per 1 nCi.

In order to obain good resolution of the ^{226}Ra alpha peak from interfering daughter products, the samples must be counted immediately after precipitation. The width of the alpha peak was found to be dependent on the sample thickness, becoming quite broad at thicknesses corresponding to 2.0 mg of Ba^{+2} as carrier(18). In the present work samples need not be prepared as carefully as required for alpha spectrometry. No detectable dependence of results on sample thickness over the range 0.5 mg to 3.5 mg of Ba^{+2} carrier was found. Interferences from other radium isotopes are easily corrected for in the present work. A further consideration when weighing the advantages and disadvantages

of a detection system is the possibility for contamination of the detector. It has previously been observed(26), using a new silicon surface barrier detector for alpha spectrometry, that the ^{222}Rn daughter products plate out on the surface of the detector, thereby increasing the background count rate. This was thought to be caused by residual radon within the counting chamber walls rediffusing into the chamber, resulting in the plate out of the radon daughters onto the detector. However, the background count rate returned to essentially zero after frequent use of the detector. This problem was not apparent in the present work over a time period of approximately one year, during which time the background counting rates for the three coincidence counting systems were checked periodically.

8.2 Improvements and Applications

The results presented in this work indicate that coincidence counting techniques provide interesting alternatives to present methods for determining ^{226}Ra concentrations in water samples. Since the suitability of coincidence counting techniques has thus been established, variations to improve the counting systems might be considered. The major drawback in performing coincidence counting is the loss in overall efficiency. If this loss in efficiency can be overcome by the use of a combination of other types of detectors, then coincidence counting could become a leading method for determining ^{226}Ra in water.

The maximum geometry obtainable with a standard NaI(Tl) detector is 2π; this condition occurs when the sample is directly on the detector face. Greater than 2 geometry is easily achieved by drilling a well into the center of the NaI(Tl) crystal, and placing the sample to be counted inside of this well. If the radioactive sample were prepared as an integral sample-scintillator mixture and combined with the NaI(Tl) well counter to form a coincidence counting system, a geometry factor approaching 4π could be achieved.

Two integral sample-scintillator arrangements are proposed; the first involves a sample-liquid scintillator mixture, and the second a, sample-ZnS(Ag) scintillation

powder mixture.

For the first method, ^{226}Ra could be precipitated from solution with $BaSO_4$, using the same procedure as given in chapter 4. The final precipitate would then be redissolved in ETDA solution to form BaEDTA and RaEDTA, since the K_{SP} values for these reactions are much greater than for the competing reactions which form $BaSO_4$, and $RaSO_4$, as discussed in section 4.2. A suitable liquid fluor would be added to the solution. This sample-liquid fluor combination would then be inserted into the NaI(Tl) well counter, and an α-γ coincidence spectrum collected.

In traditional liquid scintillation counters a two photomultiplier tube coincidence assembly is generally employed. In a coincidence arrangement, low energy beta particles from radioisotopes such as tritium are detected above the noise level. Separate channels or windows are set corresponding to specific energy regions. The technique is useful when determining counting efficiency and the degree of quenching in a sample. Quenching is generaly defined as the reduction in the efficiency of the energy transfer process in the scintillation solution, and must be determined for each type of sample counted. For the liquid scintillator-NaI(Tl) well counter coincidence system proposed here only one photomultiplier need be used because the alpha particles have enough energy to produce pulses

above the noise level in the liquid scintillator. The single photomultiplier would be positioned in the NaI(Tl) well counter behind the liquid scintillator sample. The degree of quenching and the counting efficiency must be determined from a series of calibrated ^{226}Ra solutions.

Providing that these difficulties could be overcome the NaI(Tl)-liquid fluor combination for coincidence detection of ^{226}Ra samples appears to be an attractive technique. The major gain in such a system would occur in the sample-detector geometry; a geometry factor approaching 4π could be achieved.

The second method would involve the precipitation of 226Ra with barium sulphate in the presence of scintillation grade ZnS(Ag) powder, as briefly described in section 1.2. The details of the method presented here are based on the work by D.N. Kelkar and P.V. Joshi(7). The settling of a precipitate can be accelerated if the fine particulate is absorbed on the surface of some solid materials. In this case, ZnS(Ag) was used to absorb the precipitate, since it could also be utilized for the detection of alpha particles associated with the decay of ^{226}Ra. The efficiency of counting is greatly increased for such an integral sample-scintillator arrangement. In order to precipitate the ^{226}Ra from an aqueous solution, 36 M H_2SO_4 was added dropwise, with some barium carrier, and then 400 mg of scintillation

grade ZnS(Ag) powder were added. The mixture was filtered under vaccuum onto filter discs, to give a uniformly distributed sample. The more complex precipitation procedure used in the present work, chapter 4, would not be necessary for this technique since the presence of the ZnS(Ag) powder enhances the precipitation. Initial studies of the precipitation procedure would be required in order to establish the ideal conditions for achieving maximum efficiency. These studies should include the following:

1) the chemical yield as a function of the pH;
2) the chemical yield as a function of the amount of barium carrier added;
3) the overall efficiency as a function of the amount of ZnS(Ag) powder;
4) the counting efficiency as a function of the sample thickness.

The overall efficiency including geometry was established to be 68% by Kelkar and Joshi.

To make up the two channels of a coincidence counting system, the combination sample-scintillator precipitate with a photomultiplier tube would be placed inside a NaI(Tl) well counter. The coincidence circuitry employed here would be similar to that used in the present work, as discussed in section 3.2.2. The coincidence

radiations detected would be the alpha decay of ^{226}Ra to ^{222}Rn, with the subsequent emission of the 0.186 MeV γ-ray.

An important feature for any low level ^{226}Ra detection system is that it should have the capability to be automated. In particular, the α-γ coincidence system could easily be reduced to only a few components; the NaI(Tl) detector and proportional counter with associated amplifiers, a very simple coincidence circuit, and a scaler. This simple coincidence system would be relatively low cost and easily implemented.

In order to utilize the detection capabilities of a particular counting system, extensions to determine the activities of radionuclides other than ^{226}Ra should be considered. Application of the β-γ coincidence system to the determination of ^{212}Pb activities may be possible. ^{212}Pb, also known as thorium B, is a member of the ^{232}Th decay chain, and decays to ^{212}Bi with the subsequent emission of two de-excitation γ-rays at energies of 0.239(47%), and 0.300(3.2%) MeV(13). However, if the daughter products of ^{226}Ra were also present in a sample, interferences from the de-excitation γ-rays associated with the decay of ^{214}Pb, which occur at energies of 0.295(19%), and 0.352(36%) MeV(13), would make the analysis difficult.

In conclusion, the choice of a technique for measuring ^{226}Ra concentrations in water depends on the

specific application. If high accuracy, precision, and sensitivity are required, then the radon emanation technique would be the most useful, providing that time requirements are met. If, on the other hand, it is desirable to ascertain whether a water sample is above or below a certain level of activity in order to meet government regulations for the release of radioactivity to the environment, such high precision is not required, and other methods may be considered. On the basis of the results presented in this thesis, coincidence counting techniques, particularly the α-γ coincidence technique, are viable alternatives to traditional methods for determining ^{226}Ra concentrations in water.

APPENDIX A

DETECTOR EFFICIENCY

In this section, an approximate expression for the efficiency of a detector of fixed volume V as a function of the radius, height, and absorption coefficient, is developed. The expression is then evaluated and the results are compared to tabulated values of the detection efficiency for a particular case.

From figure A.1, there are two cases to consider for a γ-ray incident on a detector with a source detector distance of d:

$$1)\ 0 \leq \theta \leq \theta_m \quad ; \ L = h/\cos\theta,$$

$$2)\ \theta_m \leq \theta \leq \theta_o \quad ; \ L = (R/\sin\theta) - (d/\cos\theta).$$

The efficiency of the detector is then given by:

$$E(R,h) = \frac{1}{2}\int_0^{\theta_m} \left(1 - e^{-h/\cos\theta} \right) \sin\theta d\theta + \int_{\theta_m}^{\theta_o} \left(1 - e^{-(R/\sin\theta - h/\cos\theta)} \right) \sin\theta d\theta$$

$$= \frac{1}{2}(1 - \cos\theta_o) - \frac{1}{2}\int_0^{\theta_m} e^{-h/\cos\theta} \sin\theta d\theta - \frac{1}{2}\int_{\theta_m}^{\theta_o} e^{-(R/\sin\theta - h/\cos\theta)} \sin\theta d\theta$$

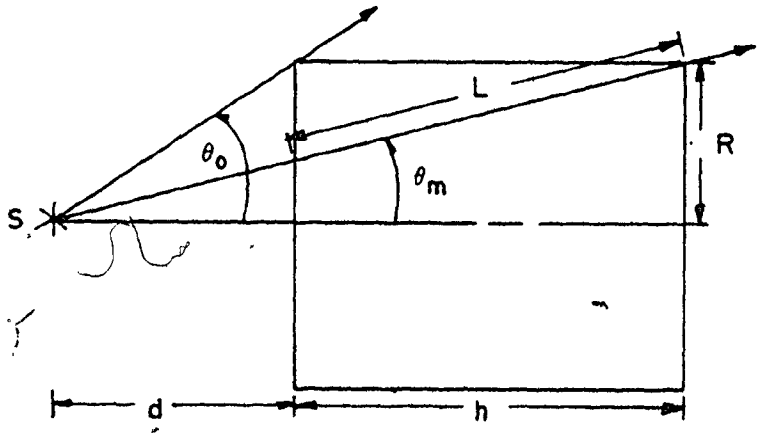

FIGURE A.1 OPTIMUM P_D DETECTOR DIMENSIONS

$$= l\,(1 - \cos\theta_o) - F_I - F_C \,.$$

If $x = \cos$, a graph of cord length = L(x) against x will yield a curve such as in figure A.2. It is possible to approximate the curves in regions 1 and 2, as shown in figure A.2, by straight lines of the form $y = ax + b$. The criteria for determining the parameters of these straight lines will be that the area under the true L(x) vs x curve must be equal to the area under the approximate straight line, with one end point fixed. Thus, for the F_C term, region 1, the area under the true L(x) curve is given by:

$$\frac{R}{\sin\theta} - \frac{d}{\cos\theta} \sin\theta d\theta = R(\theta_o - \theta_m) + d(\ln\cos\theta_o - \ln\cos\theta_m) \qquad A.1$$

and in terms of $x = \cos\theta$,

$$= R(\theta_o - \theta_m) + d(\ln x_o - \ln x_m)$$

If the cord length L(x) is approximated by a straight line $L(x) = a(x - x_o)$, where $L(x_o) = 0$, as shown in figure A.2, then the area is given by:

$$L(x)dx = \left(\frac{1}{2}ax^2 - ax_o x \right) \Big|_{x_o}^{x_m}$$

$$= a(x_m - x_o)^2 \qquad A.2$$

For the equal area criteria to be met:

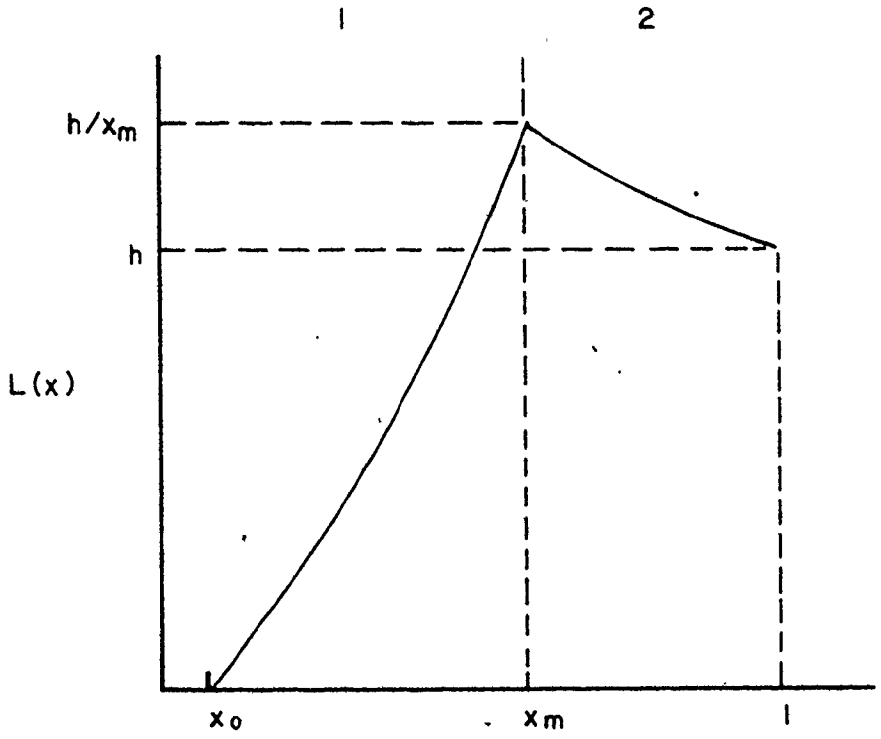

FIGURE A.2 TRUE L(x) vs x CURVE

$$a(x_m - x_o)^2 = R(\theta_o - \theta_m) + d(\ln x_o - \ln x_m) \qquad A.3$$

and therefore:

$$a = \frac{2[R(\theta_o - \theta_m) + d (\ln x_o - \ln x_m)]}{(x_m - x_o)^2} \qquad A.4$$

Thus the approximate F_C term is given by:

$$F_C = \frac{1}{2}\int_{x_o}^{x_m} e^{-\mu L(x)} dx = \frac{-1}{2\mu A} \left\{ e^{-\mu A(x_m - x_o)} - 1 \right\} , \qquad A.5$$

where:

$$A = \frac{2[R(\theta_o - \theta_m) + d (\ln x_o - \ln x_m)]}{(x_m - x_o)^2} . \qquad A.6$$

Similarily, in region 2 for the F_I term the area under the true curve L(x) is given by:

$$\int_0^{\theta_m} \frac{h}{\cos\theta} \sin\theta \, d\theta = h \ln \left\{ \frac{1}{\cos\theta_m} \right\}$$

$$= h \ln (1/x_m) \qquad A.7$$

Then if $L(x) = ax + b$, the area under the approximate curve is given by:

$$\int_{x_m}^{1} (ax + b) \, dx = \frac{1}{2} a (1 - x_m^2) + b (1 - x_m), \qquad A.8$$

and for equal areas,

$$\frac{1}{2} a (1 - x_m^2) + b (1 - x_m) = h \ln(1/x_m) \qquad A.9$$

To fix one end point such that L(x=1) = h; a + b = h. Solving these two equations for a and b yields

$$a = \frac{-2 h (\ln(1/x_m) - 1 + x_m)}{(x_m - 1)^2} \quad , \text{ and} \qquad A.10$$

$$b = h - a. \qquad A.11$$

The approximate F_I term is then given by:

$$F_I = \frac{1}{2}\int_{x_m}^{1} e^{-\mu L(x)} dx = \frac{-e^{-\mu h}}{2\mu B} \left\{ 1 - e^{-\mu B (x_m - 1)} \right\}, \qquad A.12$$

where

$$B = \frac{-2 h (\ln(1/x_m - 1 + x_m)}{(x_m - 1)^2} \qquad A.13$$

The approximate efficiency expression is then:

$E_{app}(R,h) = 1 (1 - \cos\theta_o) - F_C - F_I$, where F_C and F_I are as given above.

The above expression was tested for various values of the absorption coefficient, , for a 3"x3" (R=3.81 cm,

h=7.62 cm) detector for a source at d=10 cm. The calculated results were compared to tabulated values[17], as shown in table A.1. The approximate expression was also evaluated over a range of R and h, with fixed and varying d, and with fixed d and varying . These results are shown in figures A.3, A.4, A.5, and A.6. Figures A.3 and A.4 show the efficiency as a function of radius for two different values of .

TABLE A.1

APPROXIMATE EFFICIENCY CALCULATION

R= 3.81 cm, h= 7.62 cm, d= 10 cm

E(MeV)	$\mu(cm^{-1})$	E_{app}	E_{ref}
8.1	0.127	0.0134	0.0132
5.5	0.130	0.0136	0.0134
2.04	0.150	0.0149	0.0147
1.10	0.200	0.0177	0.0174
0.333	0.500	0.0256	0.0248
0.153	2.0	0.0309	0.0303
0.105	5.0	0.0320	0.0317
0.063	20	0.0326	0.0325
0.048	40	0.0327	0.0326
0.034	100	0.0327	0.0327

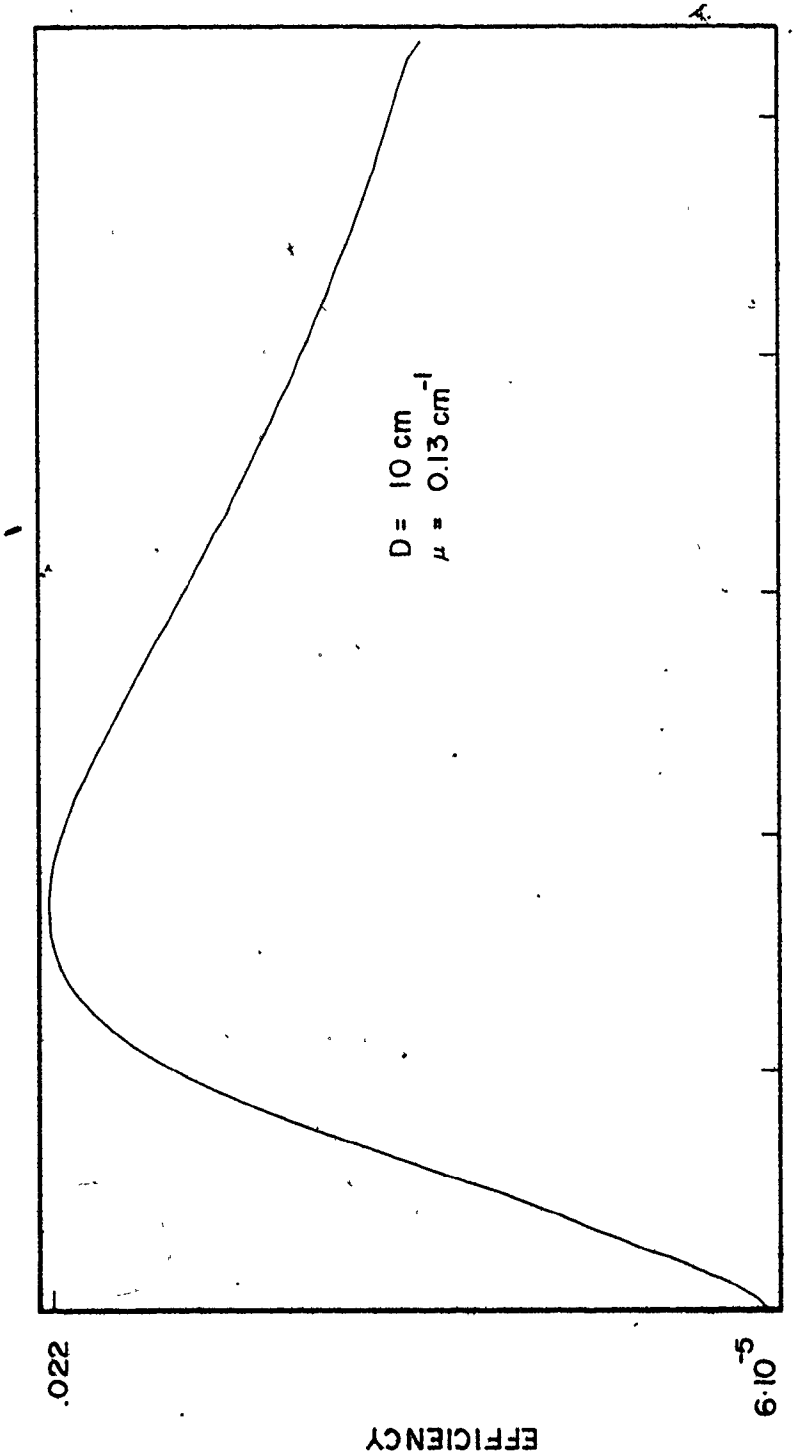

FIGURE A.3 EFFICIENCY vs RADIUS CURVE

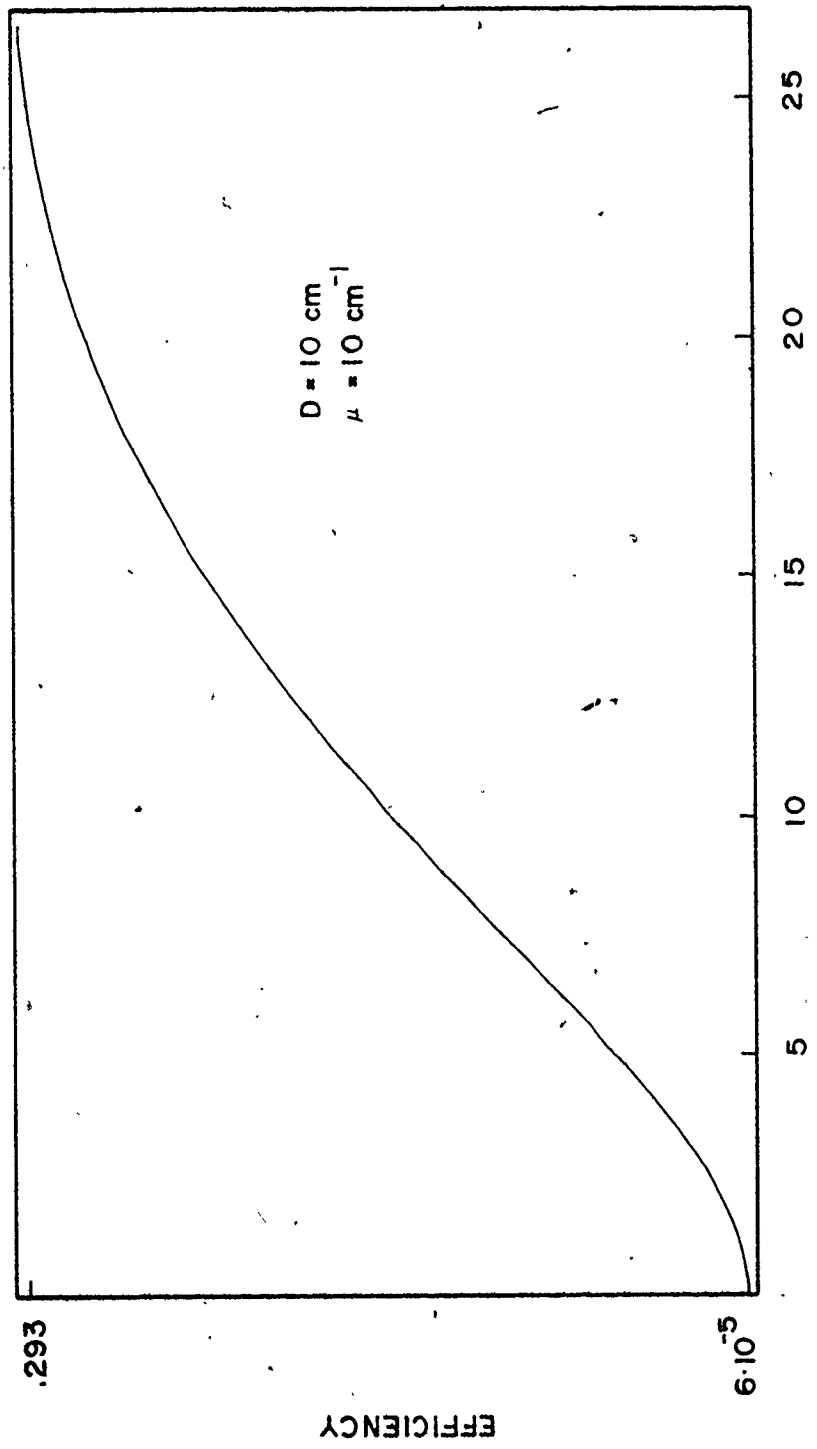

FIGURE A.4 EFFICIENCY vs RADIUS CURVE

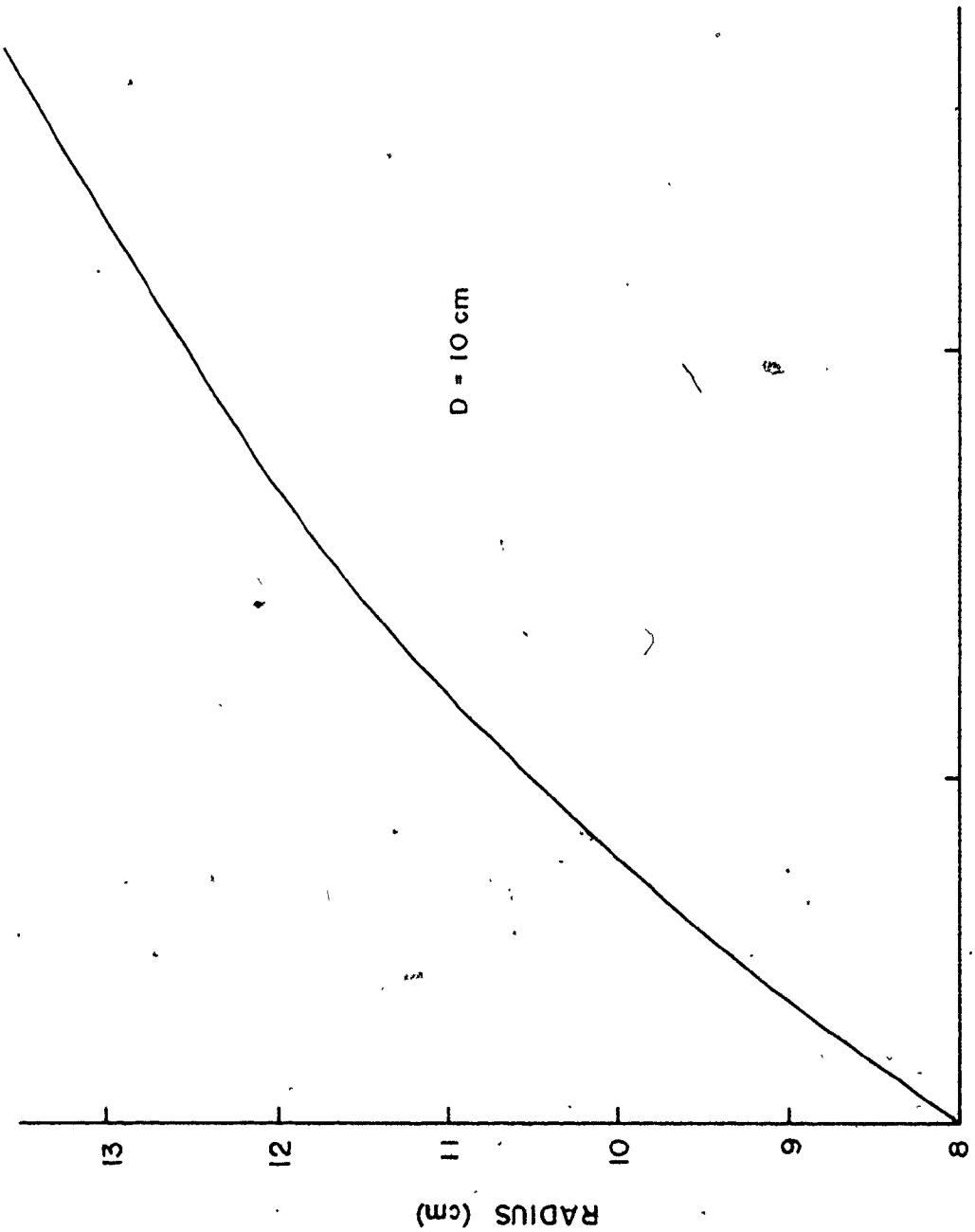

FIGURE A.5 RADIUS AT MAXIMUM EFFICIENCY vs μ AT FIXED D

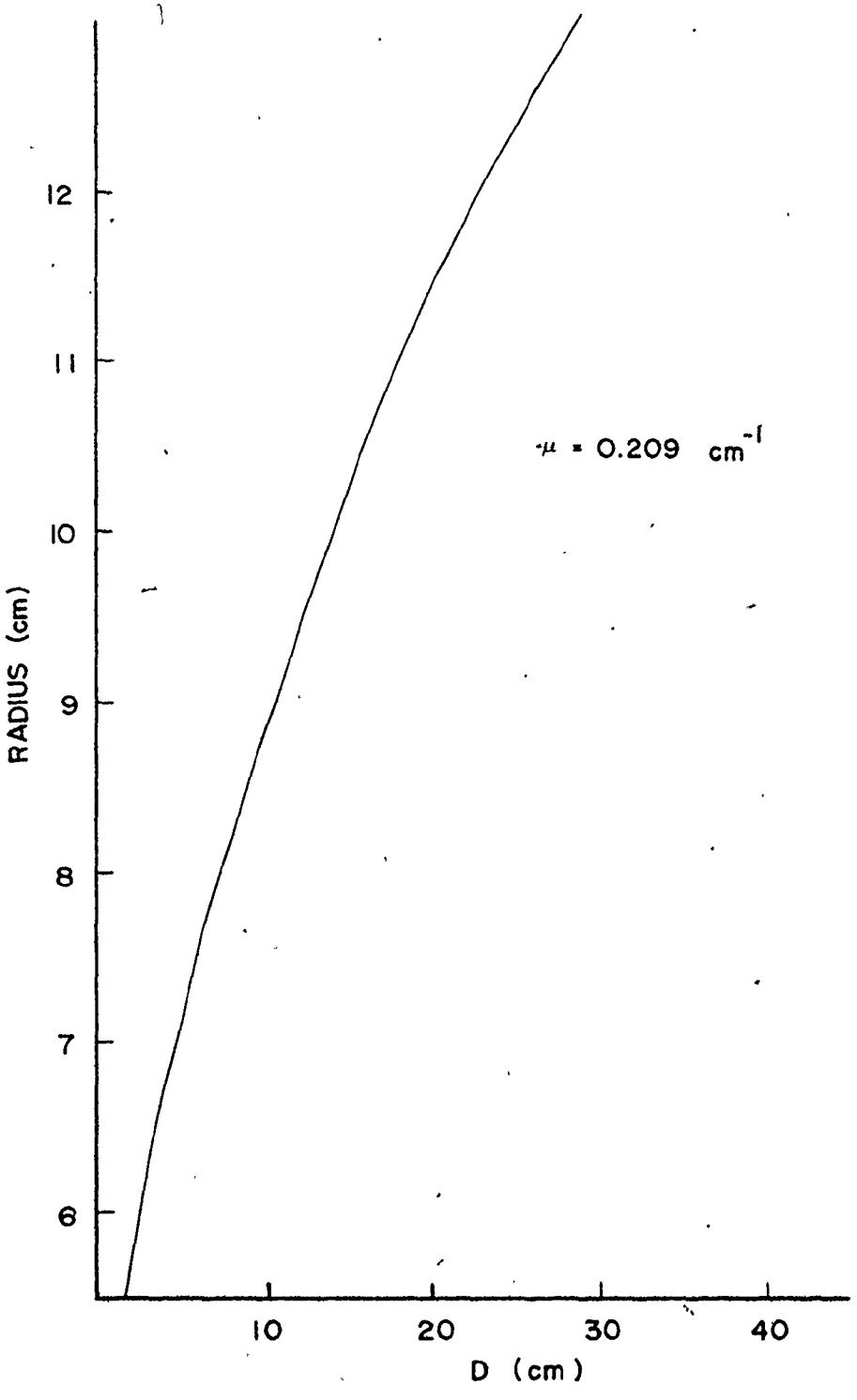

FIGURE A.6 RADIUS AT MAXIMUM EFFICIENCY vs D AT FIXED μ

REFERENCES

(1) R.D. Evans, "Radium in Man". Health Physics, Vol.27, p 497, (1974).

(2) J. Sěvc, E. Kunz, V. Plăcek, "Lung Cancer In Uranium Miners and Long Term Exposure To Radon Daughter Products". Health Physics, Vol.30, p 433, (1976).

(3) R.E. Rowland, "On the Hazards of Radium in Drinking Water". Statement, (1980).

(4) W.V. Prestwich, T.J. Kennett, "Radium Determination in Soil Samples Using A Gamma Ray Coincidence Spectrometer". Journal of Radioanalytical Chemistry, Vol.50, No.1-2, p 249, (1979).

(5) J.H. Harley, S. Forti, Nucleonics, 10(2), (1952).

(6) J.B. Zimmerman, V.C. Armstrong, "The Determination of Radium-226 in Uranium Ores and Mill Products by Alpha Energy Spectrometry". CAI MT, p 115, R11, (1976).

(7) D.N. Kelkar, P.V. Joshi, "A Rapid Method For Estimating Radium and Radon in Water." Health Physics, Vol.17, p 253, (1969).

(8) E. Pohl, J. Pohl-Rüling, "Determination of Environmental or Occupational ^{222}Rn in Air and Water and ^{226}Ra in Water With Feasible and Rapid Methods of Sampling and Measurement". Health Physics, Vol.31, p 343, (1976).

(9) R.D. Evans, Review of Scientific Instruments, 6, 99, (1931).

(10) D.E. McCurdy, R.A. Mellor, "The Application of Coincidence Counting Techniques to the Determination of ^{226}Ra and ^{228}Ra". Abstract of Talk Given at The Health Physics Society Meeting, (December, 1979).

REFERENCES

(11) A.L. Yakubovich, M.Ye. Kotsen, "Selective Analysis of Radionuclides By the Delayed Coincidence Method". J. of Radioanalytical Chemistry, Vol.57, No.2, p 461, (1980).

(12) W.V. Prestwich, T.J. Kennett, "Radium Determination in Soil Samples Using A Gamma Ray Coincidence Spectrometer". Journal of Radioanalytical Chemistry, Vol.50, No.1-2, p 249, (1979).

(13) C.M. Lederer, J.M. Hollander, I. Perlman, "Table of Isotopes", Sixth Edition, John Wiley and Sons, (1968).

(14) C.H. Wang, D.L. Willis, W.D. Loveland, "Ratiotracer Methodology in the Biological, Environmental, and Physical Sciences". Prentice Hall, (1975).

(15) K. Siegbahn, "Alpha, Beta and Gamma Ray Spectroscopy". Vol.1, North Holland Publishing Company, (1968).

(16) Tennelec Amplifier, Model TC 200, TC 907, Instruction Manual, Oak Ridge, Tennessee.

(17) F. Adams, R. Dams, "Applied Gamma-Ray Spectrometry". Second Edition, Pergammon Press, (1975).

(18) J.B. Zimmerman, V.C. Armstrong, "The Determination of Radium-226 in Uranium Ores and Mill Products by Alpha Energy Spectrometry".

(19) A. Pidruczny, Personal Communication.

(20) A. Ringbom, "Complexation in Analytical Chemistry". Chemical Analysis, Vol.16, Interscience Publishers, (1968).

(21) P.R. Bevington, "Data Reduction and Error Analysis For The Physical Sciences". McGraw-Hill, (1969).

REFERENCES

(22) H. Cramer, "Mathematical Methods Of Statistics". Princeton University Press, 12th Printing, (1971).

(23) K.A. Brownly, "Statistical Theory and Methodology In Science and Engineering". John Wiley and Sons, (1960).

(24) D.D. Slavinskas, "Mathematical Treatment of Digitized Data Containing Instrument Response and Statistical Deviations". Ph.D. Thesis, (1966).